

# On the role of trans-lithospheric faults in the long-term seismotectonic segmentation of active margins: a case study in the Andes

Gonzalo Yanez C.<sup>1</sup>, Jose Piquer R.<sup>2</sup>, Orlando Rivera H.<sup>3</sup>

<sup>1</sup> Pontificia Universidad Católica de Chile, Av. Vicuña Mackenna 4860, Macul, Santiago, Chile, gyaneza@uc.cl

<sup>2</sup> Instituto de Ciencias de la Tierra, Universidad Austral de Chile, jose.piquer@uach.cl

<sup>3</sup> Minera Peñoles de Chile, orlando\_rivera@penoles.com.mx

Correspondence to: Gonzalo Yanez C. (gyaneza@uc.cl)

**Abstract.** Plate coupling plays a fundamental role in the way in which seismic energy is released during the seismic cycle. This process includes quasi-instantaneous release during megathrust earthquakes and long-term creep. Both mechanisms can coexist in a given ~~subducting-subduction~~ margin, defining a seismotectonic segmentation in which seismically active segments are separated by zones ~~in-which~~where ruptures stop, classified for simplicity as asperities and barrier, respectively. The spatiotemporal stability of this segmentation has been a matter of debate in the seismological community for decades. At this regard, we explore in this paper the potential role of the interaction between geological heterogeneities in the overriding plate and fluids released from the subducting slab towards the subduction channel. As a case study, we take the convergence between the Nazca and South American plates between 18°-40° S, given its relatively simple convergence style and the availability of a high-quality instrumental and historical record. We postulate that trans-lithospheric faults striking at a high angle with respect to the trench behave as large fluid sinks that create the appropriate conditions for the development of barriers and promote the growth of highly coupled asperity domains in their periphery. We tested this hypothesis against key short- and long-term observations in the study area, seismological, geodetic, and geological, obtaining consistent results. If the spatial distribution of asperities is controlled by the geology of the overriding plate, seismic risk assessment could be established with better confidence.

## 1 Introduction

Subduction margins accommodate short-term (years to tens of years) and long-term (thousands to millions of years) deformation. The most evident effects of these two deformational behaviours are earthquakes (short-term) and mountain-building (long-term) (e.g. Avouac, 2007). The concept of the seismic cycle, introduced by

Código de campo cambiado

34 Fedotov (1968) and further elaborated by Mogi (1977, 1985), identifies two stages: a long inter-seismic period  
35 (several tens of years), followed by a short co-seismic period (minutes at most) where the elastic energy stored  
36 during the previous stage is released as an earthquake. For earthquake magnitudes in the range of Mw 7.5–9.5,  
37 the observed mean slip displacement varies from 0.8–10 meters (Thingbaijam et al., 2017). Even though the  
38 maximum mean slip in megathrust events is 10 meters, the zones of maximum slip, equated to asperities (e.g.,  
39 Aki, 1984, Lay & Bileck 2007, Lay 2015) can reach 20–40 meters in wavelength patches in the range of 20–  
40 100 kilometres (see, e.g., <http://equake-rc.info/srcmod/>). However, the release of elastic energy during the  
41 seismic cycle only accounts for 90-95% of the deformation accumulated interseismically in convergent margins;  
42 the remaining 5–10% produces permanent deformation in the overriding plate, expressed as crustal shortening  
43 and mountain building (e.g. Yañez and Cembrano, 2004). This long-term process lasts for hundreds to  
44 thousands of seismic cycles (time windows of millions of years). Therefore, both phenomena — earthquakes  
45 and mountain building — are extreme responses to the same process: the convergence between oceanic and  
46 continental plates.

47 The concepts of asperities and barriers were proposed by Lay et al. (1982) and Aki (1984) to describe the  
48 process during the occurrence of an earthquake and intimately related to the concept of plate coupling. More  
49 recent studies (e.g. Bileck and Lay, 2007) propose a more complex mechanism at the subduction plate contact,  
50 in which domains of unstable stick-slip state coexist with other domains in a conditionally stable stick-slip state,  
51 and zones that develop aseismic slip/stable behaviour. These three states — unstable, conditionally stable, and  
52 stable stick-slip behaviour — represent different slip modes that can be represented as asperities and barriers in  
53 the old nomenclature (Scholz, 1990). However, the conceptualization of Bileck and Lay (2007) proposes an  
54 ~~along~~down-dip (depth) distribution of the different slip behaviours: (1) aseismic-stable at depths of 5–10  
55 kilometres, (2) mostly conditionally stable at depths of 10–15 kilometres, and (3) unstable stick-slip behaviour  
56 (Brace and Byerlee (1966) and Burridge and Knopoff (1967)) at depths of 15–25 kilometres. Recent studies on  
57 exhumed subduction domains in California (Platt et al., 2018) corroborate this ~~along~~down-dip transition from  
58 seismic zone to transition zone. One interesting characteristic of these domains is that unstable domains are  
59 generally surrounded by conditionally stable domains and aseismic domains in their outermost periphery.

60 To date, there is no clear evidence on whether the geological/tectonic process(es) control to some extent these  
61 seismogenic behaviours and/or their stability across several seismic cycles or geological time frames. Potential  
62 candidates already proposed include: (1) the roughness of the subducting plate (aseismic ridges, fracture zones,  
63 horst/graben structures, etc.) (e.g. Bilek et al., 2003, Wang and Bilek, 2011; Gersen et al., 2015; Philibosian and  
64 Meltzner, 2020; Molina et al., 2021); (2) fluid-controlled overpressure (Peacock, 1990; Safer and Tobin, 2011;  
65 Safer, 2017; Menant et al., 2019); (3) the shape of the subducting plate (e.g. Gutscher et al., 1999); (4) the  
66 geology of the overriding plate (i.e Kimura et al., 2018; Philibosian and Meltzner, 2020; Molina et al., 2021),  
67 among others, including various combinations of these different possible factors.

68 The role of fluids released from the subducting slab has emerged as a first-order factor in the plate-coupling  
69 processes at subduction margins. Direct observations (e.g., Saffer and Tobin, 2011; Tsuji et al., 2014, Moreno  
70 et al., 2014) and numerical modelling (Menant et al., 2019) demonstrate that fluids released from the subducting  
71 oceanic crust and subduction channel define segments at the plate-coupling zone with distinct pore pressure

72 characteristics. Overpressure domains are associated with zones of weak coupling, and strong coupling is  
73 observed in the case of zones showing low pore pressure behaviour. The first type of domain is in direct  
74 association with creep zones or slow slip events, while the other one is in direct association with locked zones,  
75 or in the seismological nomenclature, the barrier and asperity domains, respectively. Seismic imaging of the  
76 forearc wedge (e.g. Tsuji et al., 2014) and numerical modelling also show that fluids percolate upwards in the  
77 zones of maximum overpressure, including the emplacement of serpentinite bodies along weak zones or faults.  
78

79 In this paper, we propose a causal relationship between the presence of trans-lithospheric faults (TLF) in the  
80 overriding plate and seismic segmentation, involving the control of TLF on the movement/storage/release of  
81 overpressure fluids along and across the subduction zone. We use the Central Southern Andes as a case study,  
82 as it is one of the most active seismogenic sites worldwide, is well studied, and has a relatively simple  
83 subduction geometry (Hayes, 2018). In addition, recent structural and geophysical mapping has revealed the  
84 role of TLF in the tectono-magmatic evolution of the continental margin of this region (e.g. Yáñez et al., 1988,  
85 Santibáñez et al., 2019; Cembrano and Lara, 2009; Melnick and Echtler, 2006; Yáñez and Rivera, 2019; Piquer  
86 et al., 2019, 2021a). We aim to demonstrate that the interaction between these TLF and the fluid circulating  
87 through the subduction channel provides a simple first-order explanation for the Andean seismotectonic  
88 organization through a long-lived geological control.

## 89 **2 Data and methods**

### 90 **2.1 Tectonic background**

91 The Nazca-South American plate convergence is a subduction-type margin that has been active in this segment  
92 of the Andes since at least the Cretaceous without the accretion of new terrains (Mpodozis and Ramos, 1990).  
93 Since 15 Ma, the convergence has been slightly oblique (E10°N) at a velocity of around 6.5 cm/yr (Angermann  
94 et al., 1999). The age of the oceanic plate varies between 0 Ma at the triple junction of Taitao (44°S) to 45 Ma  
95 at the Orocline bending of Bolivia (18°S) (Figure 1). A flat slab segment is located between 28°S and 33°S  
96 latitude, affecting the development of an asthenospheric wedge landward and inhibiting the occurrence of active  
97 volcanism since the last 5 Ma (Kay and Mpodozis, 2002). However, the Wadati-Benioff plane is roughly  
98 homogenous in dip along the plate coupling boundary between the Nazca and South American plates (Slab 2.0,  
99 Hayes, 2018). The roughness of the Nazca plate is affected by a progressively older oceanic crust northward,  
100 with some fracture zones offsetting the plate, the subduction of a triple junction with an active spreading centre  
101 (now at Taitao Peninsula), some episodic magmatic activity along the Juan Fernandez Ridge (33°S, Yáñez et  
102 al., 2001), and eventually a smaller ridge at 20°S (Perdida Ridge, Cahill and Isacks, 1992). Overall, these  
103 features can be described as minor obstacles to the subduction of a relatively young oceanic plate underneath a  
104 continental plate in a highly coupled convergence convergent margin (Section 2.5).  
105

106 **2.2 Compilation of trans-lithospheric faults in the Andean active margin and their role as long-lived**  
107 **high-permeability domains**

108 Trans-lithospheric faults (TLF) correspond to long-lived, high-angle fault systems, which have been identified  
109 in several segments of the Andean margin, based on geological mapping (e.g. Santibañez et al. 2019; Cembrano  
110 and Lara, 2009; Melnick and Echtler, 2006; Piquer et al., 2021a; Farrar et al., 2023; Wiemer et al., 2023), crustal  
111 seismicity (e.g. Talwani, 2014.), a combination of indirect geophysical techniques (Yañez et al., 1998), or a  
112 combination of all of these (Yañez and Rivera, 2019; Piquer et al., 2019; Pearce et al., 2020). The geometry and  
113 depth extension of TLF is unknown, but based on their control of the continental-scale magmatic and  
114 hydrothermal processes and their surface traces in the order of hundreds of kms, we consider that they involve,  
115 exclusively, the whole lithosphere.

116 In Table 1 we present a synthesis of the current status of knowledge regarding TLF definition and the major  
117 geological/geophysical evidences that described them. The number assigned in each case is used later on in  
118 Figure 1 as an identificatory.

119 Detailed structural mapping in various segments of the Andean margin has provided direct geological evidence  
120 for the presence of TLF. They are manifested in the field as networks of individual high-angle faults, defining  
121 deformation zones with widths of up to several kilometres, and lengths in the order of hundreds of kilometres,  
122 being possible to follow their trace across the entire continental margin (Lanza et al., 2013; Yañez and Rivera,  
123 2019; Piquer et al., 2021a). These fault networks correspond to the expression at the present-day surface of a  
124 pre-existing TLF, as a result of its vertical propagation through Mesozoic and Cenozoic igneous and  
125 sedimentary rocks (McCuaig and Hronsky, 2014; Piquer et al., 2019). Field observations also show that,  
126 consistent with their high dip angle (commonly  $>60^\circ$  and in several cases sub-vertical, although individual fault  
127 segments can dip at slightly lower angles), TLF tend to be reactivated as basin-bounding faults during  
128 extensional episodes, and are thus associated with ~~violet-sharp~~ changes in the stratigraphic record (Piquer et  
129 al., 2015, 2021a; Yañez and Rivera, 2019). They also control the distribution of exhumed basement blocks  
130 (Yañez and Rivera, 2019).

131 The geological record demonstrates that TLF are long-lived structures, ~~which-that~~ have played a major role in  
132 the long-term evolution of the Chilean continental margin, being reactivated with different kinematics under  
133 varying tectonic regimes. It is likely that several TLF were originated in the Proterozoic and the Palaeozoic  
134 (Yañez and Rivera, 2019); there is strong geological evidence suggesting the present-day TLF architecture was  
135 already in place by the Permo-Triassic, a period in which these structures acted as master and transfer faults for  
136 intra-continental rift systems (Niemeyer et al., 2004; Sagripanti et al., 2014; Espinoza et al., 2019). Syn-tectonic  
137 emplacement of magma along TLF has been documented at least since the Jurassic (Creixell et al., 2011).

138 Geophysical support for the TLF architecture in the continental margin is provided by the geometry of magnetic  
139 and gravimetric anomalies (Piquer et al., 2019; Yañez and Rivera, 2019) and also by magnetotelluric data  
140 (Pearce et al., 2020) and seismic tomography (Yañez and Rivera, 2019). Evidence of seismic activity in some  
141 of these TLF has been recorded, for example, a precursory event to the 9.3 Mw 1960 Valdivia Earthquake  
142 (Lanahue fault, Melnick et al., 2009), and the coseismic rebound associated with the 8.8 Mw 2010 Maule  
143 earthquake (Pichilemu fault, e.g. Farías et al, 2011; Aron et al., 2013). Additionally, researchers have

144 documented a strong spatial relationship between a TLF and a major seismic swarm (Valparaíso seismic  
145 sequence of 2017, Nealy et al., 2017) at the subduction megathrust (Piquer et al., 2021a).

146 Regarding the role of TLF as long-lived high-permeability domains, Yañez and Rivera (2019) postulated that  
147 they represent weak lithospheric domains that favour fluid flow and the emplacement of different types of ore  
148 deposits over large time periods (tens of millions of years), beginning with stratabound and IOCG-type deposits  
149 in the Jurassic. A similar conclusion has been reached by Farrar et al. (2023) for the emplacement of porphyry  
150 copper deposits of various ages, and by Wiemer et al. (2023) for gold-rich superclusters of various types of  
151 mineral deposits. The strong relationship between the locations of TLF and those of giant ore deposits at specific  
152 metallogenic belts has been discussed more specifically in the Andes of Northern (e.g., Chernicoff et al., 2002)  
153 and Central Chile (e.g., Piquer et al., 2016) and neighbouring regions in Argentina. Similarly, there is a well-  
154 established relationship between the locations of TLF and volcanic/geothermal activity in the Andes of Southern  
155 Chile (e.g., Cembrano and Lara, 2009). Moreover, high Vp/Vs ratios that were documented during the  
156 Pichilemu seismic sequence following the 2010 Maule earthquake have been interpreted as strong evidence of  
157 fluid migration (Farías et al., 2011, Calle-Gardella et al., 2021).

158 Various authors have discussed how the type of magmatic-hydrothermal product and fluid flow regime varies  
159 depending on the orientation of a specific high-angle fault system (in several cases, a TLF) relative to the  
160 predominant stress tensor (Lara et al., 2006; Cembrano and Lara, 2009; Roquer et al., 2017; Piquer et al.,  
161 2021b). Of particular relevance is the orientation of the fault system relative to the maximum stress ( $\sigma_1$ ); if the  
162 fault system is sub-parallel or strikes at a low angle relative to  $\sigma_1$ , it is well-oriented for opening and reactivation  
163 respectively, allowing the rapid ascent of magma and hydrothermal fluids through different crustal segments.  
164 On the other hand, if the fault system is sub-perpendicular or strikes at a high angle relative to  $\sigma_1$ , it would be  
165 poorly oriented or misoriented for reactivation and would promote the storage of magma and hydrothermal  
166 fluids at depth (e.g. Cembrano and Lara, 2009; Stanton-Yonge et al., 2016; Piquer et al., 2021b). In the latter  
167 case, a requirement for fault reactivation and the release of the accumulated fluids is that supra-lithostatic fluid  
168 pressures are achieved; once this occurs, the fault system would allow the discharge of the accumulated fluids  
169 towards upper crustal levels and would act as a fluid pump (“fault-valve behaviour”), concentrating fluids in  
170 the fractured areas within the fault system and leading to the depletion of fluids in the surrounding regions  
171 (Sibson, 1990, 2020; Cox, 2016). These fluid discharge events cause seismic swarms (Cox, 2016), which  
172 concentrate at the base of the high-angle fault system (Sibson, 2020).

173 Figure 1 presents the main array of NW- and NE-striking TLF observed in the Andean margin; their seaward  
174 trend has been extrapolated following the observed trend in the continental lithosphere, in particular south of  
175 36°S, following the trace of submarine canyons.

176

177 Table 1: Main Trans-Lithospheric Faults of the Chilean Andes (17-42°S Latitude)  
178

LSS_ID	LSS_NAME	REFERENCES	GEOLOGICAL EVIDENCES
1	Visviri	(15), (22)	(L)(TLS)(SC)(GVA), Antofalla Basement (T)
2	Arica	(15), (21), (22)	Arequipa Massif (T), ETL NW Arica (TLS)
3	Camarones	(22)	(TLS)(GVA)(SDGU)
4	Iquique	(22)	(TLS)(GVA)(SDGU)
5	Calama	(1), (2), (8), (20), (21), (22), (24)	Comache (F), Calama-Olacapato-EI Toro (L)(FS)(VA), Solá (F), Chorrillos (F), ETL NW Calama (TLS)
6	Mejillones-Llullaillaco	(8), (10), (21), (22), (29), (35)	Archibarca (L)(VA), Cataclásitas de Sierra de Varas (DZ), ETL NW Mejillones (TLS), Socompa (FS)
7	Agua Verde-Exploradora	(8), (22)	Culampajá (L)
8	Antofagasta-Conchi	(22), (27), (28), (30)	Antofagasta-Calama (L)(PMG)(TR)(STMH)
9	Taltal-Potrerrillos	(8), (22)	Taltal (L)(TLS)(SDGU)(VA)(STMH)
10	Chañaral	(8), (22)	(TLS)(GVA)(SDGU)
11	Copiapó	(22)	(TLS)(SDGU)
12	Vallenar	(22)	(TLS)(SDGU)
13	Domeyko	(22), (36)	(TLS)(GVA)(SDGU), Cruzadero (F)
14	Vicuña	(22)	(TLS)(GVA)(SDGU)
15	Andacollo	(22)	(TLS)(GVA)(SDGU)(STMH)
16	Punitaqui-Los Pelambres	(22)	(TLS)(GVA)(SDGU)(MA)(STMH)
17	El Potro	(22)	(TLS)(SDGU)
18	Illapel	(22)	(TLS)(GVA)(SDGU)
19	Almendrillo	(22)	(TLS)(GVA)(SDGU)
20	La Ligua-Los Andes	(21), (22), (31)	(TLS)(GVA)(SDGU)(SC)(MA), Río Blanco-Los Bronces (FS)(STMH)
21	Valparaíso-Volcán Maipo	(3), (5), (7), (19), (21), (22), (23), (26)	Piuquencillo (F)(FS)(STMH), Melipilla (F)(MA), Marga-Marga (FS), Valparaíso-Curacaví (FS)(STMH), Concón (MDS), Cartagena (MDS), El Tabo (MDS)
22	Pichilemu	(9), (17), (22), (23), (24), (25)	Pichilemu (ATS), Tenó (FS)(SC)(STMH), Planchón-Peteroa (LLBS)(SC)
23	Laguna del Maule	(32), (33)	Río Maule (F)(VA)(SDGU)(STMH)
24	Iloca-Río Melado	(34)	Laguna Fea (FS)(VA)(STMH)
25	Aconcagua-San Antonio	(4), (6), (22), (23), (31)	Puangué (F), Estero Chacabuco (F), Estero Colina (F), El Salto (FS)(STMH)
26	Volcán Quizapu	(33)	(VA)(MDS)
27	Parral-Bullileo	This study	(VA)(SDGU)
28	San Carlos-Nevedos de Chillán	(12), (17), (18)	Chillán (AZ), Nevados de Chillán-Tromén (LLBS), Cortaderas (L)
29	Lanahue-Volcán Villarrica	(11), (14), (16), (17), (24)	Morguilla (FLS), Lanahue (F)(FS), Villarrica-Quetrupillán-Lanín (LLBS)
30	Tirúa-Pitrufquén	(11), (16)	Mocha-Villarrica (FS)
31	Río Calle Calle-Lago Ranco	(13), (17)	Carrán-Los Venados (LLBS), Futrono (F)
32	Puerto Saavedra-Volcán Callaqui	(18)	Copahue-Callaqui (AZ)
33	Osorno-Volcán Calbuco	This study	(VA)
34	Ancud-Volcán Michimahuida	(17)	Michimahuida (LLBS)
35	Cucao-Chaitén	(17)	Chaitén (LLBS)
36	Chacao-Osorno-Puntiagudo	(17)	(VA)

**Abbreviations:** (ATS) Andean Transverse System; (AZ) Accommodation Zone; (DZ) Deformation Zone; (F) Fault; (FLS) Fault-line Scarp; (FS) Fault System; (GVA) Gravimetric Anomaly; (L) Lineament; (LLBS) Long-Lived Basement Structures; (LLTF) Long-Lived Transverse Fault; (MA) Magnetic Anomaly; (MDS) Mafic Dike Swarm; (PMG) Paleomagnetism; (SC) Seismic Cluster; (SDGU) Structural Discontinuity of Geological Units; (T) Terrane; (TLS) Translithospheric Structures; (TR) Tectonic Rotations; (STMH) Syn-Tectonic Magmatic-Hydrothermal Centers; (VA) Volcano Alignment.

**Reference Keys:** (1) Salfity, 1985; (2) Marrett et al., 1994; (3) Gana et al., 1996; (4) Wall et al., 1996; (5) Yáñez et al., 1998; (6) Wall et al., 1999; (7) Rivera & Cembrano, 2000; (8) Chernicoff et al., 2002; (9) Sernageomin, 2003; (10) Niemeyer et al., 2004; (11) Haberland et al., 2006; (12) Ramos & Kay, 2006; (13) Lara et al., 2006; (14) Glodny et al., 2008; (15) Ramos, 2008; (16) Melnick et al., 2009; (17) Cembrano & Lara, 2009; (18) Radic, 2010; (19) Creixell et al., 2011; (20) Lanza et al., 2013; (21) Rivera, 2017; (22) Yáñez & Rivera, 2019; (23) Piquer et al., 2019; (24) Santibáñez et al., 2019; (25) Pearce et al., 2020; (26) Piquer et al., 2021a; (27) Arriagada et al., 2003; (28) Peña, 2010; (29) Richards et al., 2013; (30) Palacios et al., 2007; (31) Piquer et al., 2015; (32) Kohler, 2016; (33) Fischer, 2021; (34) Torres, 2021; (35) Farrar et al., 2023; (36) Giambiagi et al., 2017.

LSS_ID	LSS_NAME	REFERENCES	GEOLOGICAL EVIDENCES
1	Visviri	(15), (22)	(L)(TLS)(SC)(GVA), Antofalla Basement (T)
2	Arica	(15), (21), (22)	Arequipa Massif (T), ETL NW Arica (TLS)
3	Camarones	(22)	(TLS)(GVA)(SDGU)
4	Iquique	(22)	(TLS)(GVA)(SDGU)
5	Calama	(1), (2), (8), (20), (21), (22), (24)	Comache (F), Calama-Olacapato-EI Toro (L)(FS)(VA), Solá (F), Chorrillos (F), ETL NW Calama (TLS)
6	Mejillones-Llullaillaco	(8), (10), (21), (22), (29), (35)	Archibarca (L)(VA), Cataclasis de Sierra de Varas (DZ), ETL NW Mejillones (TLS), Socompa (FS)
7	Agua Verde-Exploradora	(8), (22)	Culampajá (L)
8	Antofagasta-Conchi	(22), (27), (28), (30)	Antofagasta-Calama (L)(PMG)(TR)(STMH)
9	Taltal-Potrerillos	(8), (22)	Taltal (L)(TLS)(SDGU)(VA)(STMH)
10	Chañaral	(8), (22)	(TLS)(GVA)(SDGU)
11	Copiapó	(22)	(TLS)(SDGU)
12	Vallenar	(22)	(TLS)(SDGU)
13	Domeyko	(22), (36)	(TLS)(GVA)(SDGU), Cruzadero (F)
14	Vicuña	(22)	(TLS)(GVA)(SDGU)
15	Andacollo	(22)	(TLS)(GVA)(SDGU)(STMH)
16	Punitaqui-Los Pelambres	(22)	(TLS)(GVA)(SDGU)(MA)(STMH)
17	El Potro	(22)	(TLS)(SDGU)
18	Illapel	(22)	(TLS)(GVA)(SDGU)
19	Almendrillo	(22)	(TLS)(GVA)(SDGU)
20	La Ligua-Los Andes	(21), (22), (31)	(TLS)(GVA)(SDGU)(SC)(MA), Río Blanco-Los Bronces (FS)(STMH)
21	Valparaíso-Volcán Maipo	(3), (5), (7), (19), (21), (22), (23), (26)	Piñuquillo (F)(FS)(STMH), Melipilla (F)(MA), Marga-Marga (FS), Valparaíso-Curacavi (FS)(STMH), Concón (MDS), Cartagena (MDS), El Tabo (MDS)
22	Pichilemu	(9), (17), (22), (23), (24), (25)	Pichilemu (ATS), Teno (FS)(SC)(STMH), Planchón-Peteroa (LLBS)(SC)
23	Laguna del Maule	(32), (33)	Río Maule (F)(VA)(SDGU)(STMH)
24	Iloca-Río Melado	(34)	Laguna Fea (FS)(VA)(STMH)
25	Aconcagua-San Antonio	(4), (6), (22), (23), (31)	Puangue (F), Estero Chacabuco (F), Estero Colina (F), El Salto (FS)(STMH)
26	Volcán Quizapu	(33)	(VA)(MDS)
27	Parral-Bullileo	This study	(VA)(SDGU)
28	San Carlos-Nevedos de Chillán	(12), (17), (18)	Chillán (AZ), Nevados de Chillán-Tromen (LLBS), Cortaderas (L)
29	Lanahue-Volcán Villarrica	(11), (14), (16), (17), (24)	Morguilla (FLS), Lanahue (F)(FS), Villarrica-Quetripillán-Lanín (LLBS)
30	Tirúa-Pitrufquén	(11), (16)	Mocha-Villarrica (FS)
31	Río Calle Calle-Lago Rancho	(13), (17)	Carrán-Los Venados (LLBS), Futrono (F)
32	Puerto Saavedra-Volcán Callaqui	(18)	Copahue-Callaqui (AZ)
33	Osorno-Volcán Calbuco	This study	(VA)
34	Ancud-Volcán Michimahuida	(17)	Michimahuida (LLBS)
35	Cucao-Chaitén	(17)	Chaitén (LLBS)
36	Chacao-Osorno-Puntiagudo	(17)	(VA)

**Abbreviations:** (ATS) Andean Transverse System; (AZ) Accommodation Zone; (DZ) Deformation Zone; (F) Fault; (FLS) Fault-line Scarp; (FS) Fault System; (GVA) Gravimetric Anomaly; (L) Lineament; (LLBS) Long-Lived Basement Structures; (LLTF) Long-Lived Transverse Fault; (MA) Magnetic Anomaly; (MDS) Mafic Dike Swarms; (PMG) Paleomagnetism; (SC) Seismic Cluster; (SDGU) Structural Discontinuity of Geological Units; (T) Terrane; (TLS) Translithospheric Structures; (TR) Tectonic Rotations; (STMH) Syn-Tectonic Magmatic-Hydrothermal Centers; (VA) Volcano Alignment.

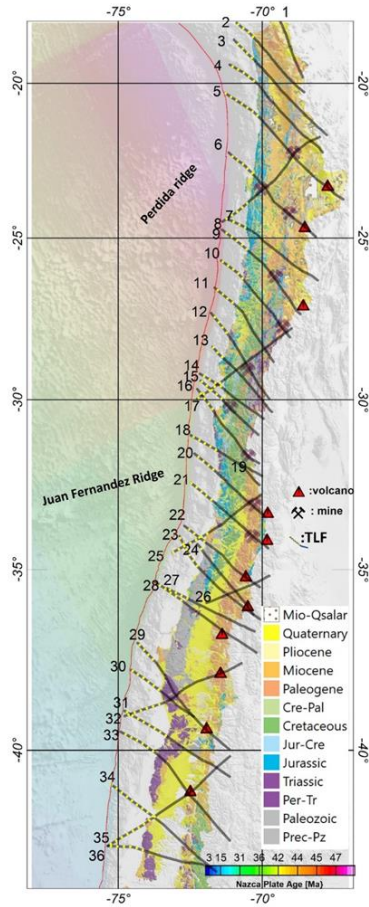
**Reference Keys:** (1) Salfity, 1985; (2) Marrett et al., 1994; (3) Gana et al., 1996; (4) Wall et al., 1996; (5) Yáñez et al., 1998; (6) Wall et al., 1999; (7) Rivera & Cembrano, 2000; (8) Chernicoff et al., 2002; (9) Sernageomin, 2003; (10) Niemeyer et al., 2004; (11) Haberland et al., 2006; (12) Ramos & Kay, 2006; (13) Lara et al., 2006; (14) Glodny et al., 2008; (15) Ramos, 2008; (16) Melnick et al., 2009; (17) Cembrano & Lara, 2009; (18) Radic, 2010; (19) Creixell et al., 2011; (20) Lanza et al., 2013; (21) Rivera, 2017; (22) Yáñez & Rivera, 2019; (23) Piquer et al., 2019; (24) Santibáñez et al., 2019; (25) Pearce et al., 2020; (26) Piquer et al., 2021a; (27) Arriagada et al., 2003; (28) Peña, 2010; (29) Richards et al., 2013; (30) Palacios et al., 2007; (31) Piquer et al., 2015; (32) Kohler, 2016; (33) Fischer, 2021; (34) Torres, 2021; (35) Farrar et al., 2023; (36) Giambiagi et al., 2017.

180

181

182





183

184

185

186

187

188

189

190

191

192

193

194

Figure 1: The spatial distribution of trans-lithospheric faults (TLF) over the regional geology of the Chilean continental margin (from SERNAGEOMIN, 2003). The traces of the TLF's are based on the models of Yáñez and Rivera (2019) and Piquer et al. (2019) in Northern and Central Chile, and after the model of Melnick and Echlter (2006) in Southern Chile. Also shown are the locations of the main ore deposits (from north to south, Chuquicamata, Mantos Blancos, Escondida, Salvador, Cerro Casale, El Indio, Andacollo, Los Pelambres, Río Blanco-Los Bronces and El Teniente), and active volcanoes (from north to south, Lásca, Lullaillaco, Ojos del Salado, Tupungatito, Maipo, Planchón-Peteroa, Laguna del Maule, Chillán, Callaqui, Villarrica and Osorno) to show their correspondence with the TLF array. TLF are extended until the trench, following their main trend and the canyons trace to the south of 36°S, using segmented red lines to highlight the uncertainty of this offshore extension. In the seaward side of the figure, the age map of Müller et al. (2019) is included with the bathymetry of the seafloor.

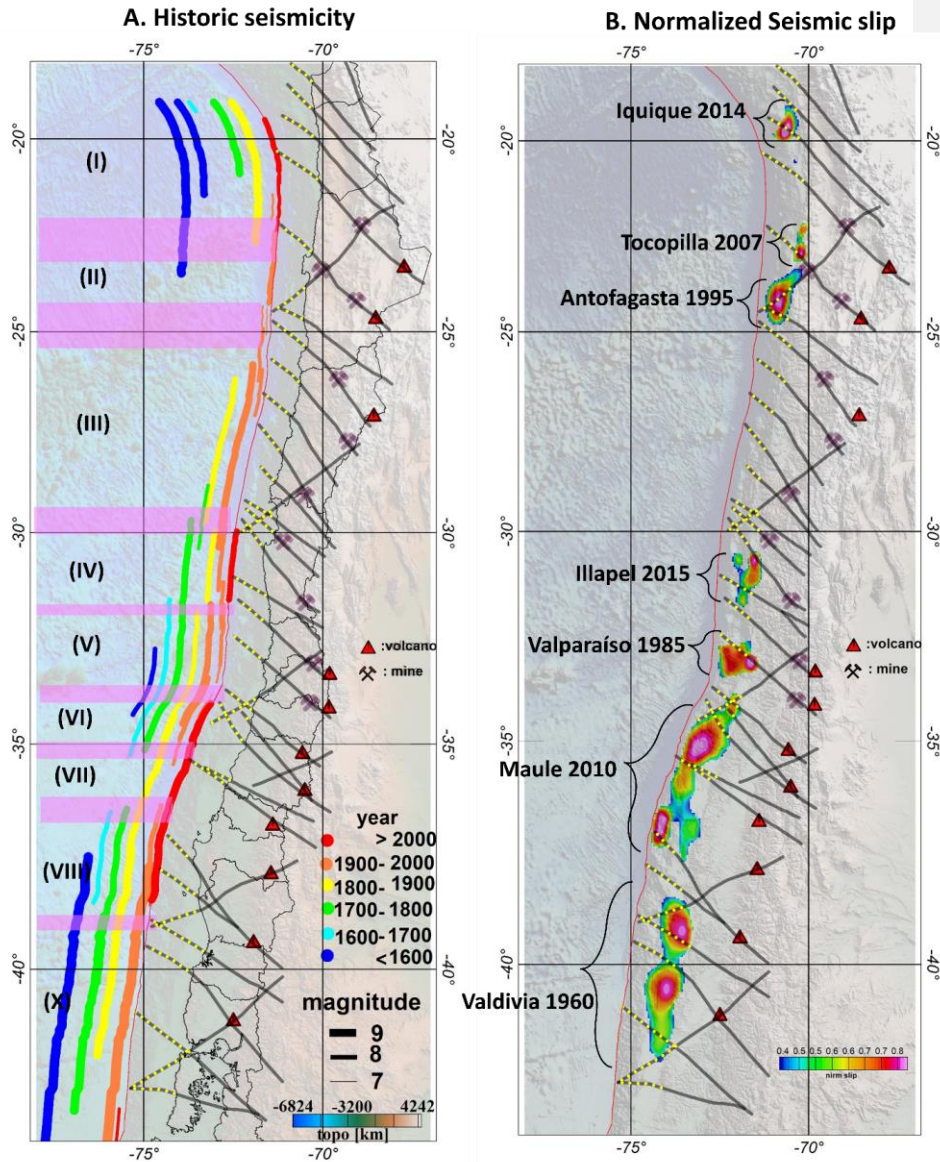
195 **2.3 Historic subduction seismicity and Slip solutions during the last 50 years and Trans-lithospheric**  
196 **faults (TLF) correspondance**

197 The historic seismic record in the region is short, extending from the start of the Spanish Colonization in the  
198 region (present territories of Perú and Chile, circa 1500 ac). Compilations of historic seismicity and subsequent  
199 interpretation to assess the magnitude and longitudinal extension of the events have been provided in Ruiz and  
200 Madariaga (2018) and Scholz and Campos (2012), among others. Figure 2, panel A, includes all the historic  
201 events described by these authors, as well as events above 7 Mw from the USGS catalogue. As noted by several  
202 authors (Ruiz and Madariaga, 2018, and references therein), there is evidence of seismo-tectonic segmentation  
203 in the historic record. For the present analysis, we define seven domains from north to south; the boundary  
204 between domains is defined by a region of roughly 100-200 kilometres that represents the uncertainty in the  
205 rupture length of the major events. We consider wider boundaries for the cases of lacking information, in  
206 particular in the northern area where the historic record is scarce. Domain I, in the northernmost part of the  
207 study region, shows a sequence of events close to magnitude 8 Mw and separated by 100–150 years. Domain  
208 II has no large events (above 8 Mw) in the historic record, instead having a series of intermediate events of  
209 magnitude 7–7.7 Mw between 1960 and 2020. Domain III has two events with magnitudes in the range 8.3–8.5  
210 Mw separated by almost 10 years, but with a current seismic gap of 100 years. Domain IV is less than 200  
211 kilometres in length and includes a series of seismic events of magnitude 8 Mw or above. According to Ruiz  
212 and Madariaga (2018), the three major events in this domain show relatively consistent recurrence times (60–  
213 80 years) and magnitudes (8–8.4 Mw), namely, the earthquakes of 2015 (Illapel, 8.3 Mw), 1943, and 1880.  
214 Domain V is also relatively small, about 300 km, and includes regular events of around magnitude 8 Mw,  
215 including the Valparaiso 1985 8 Mw event and the 1906 8.4 Mw event. Domain VI, VII and VIII include part  
216 of the Maule 2010 8.8 Mw and Concepción 1835 8.6 Mw events, but are defined as such based on some less  
217 than 8 Mw events, Domain X, the southernmost domain, is dominated by the giant events of Valdivia 1960, 9.5  
218 Mw, and 1737, 9.0 Mw.

219 Adequate seismic coverage is available since 1985 in Chile. In this period, six large earthquakes have been  
220 recorded: Valparaiso 1985, 8.0 Mw (Comte et al., 1986; Mendoza et al., 1994); Antofagasta 1995, 8.0 Mw  
221 (Ruegg et al., 1996, Delouis et al., 1997; Pritchard et al., 2002 and Chlieh et al., 2004); Tocopilla 2007, 7.8 Mw  
222 (Schurr et al., 2012); Maule 2010, 8.8 Mw (Delouis et al., 2010; Lay et al., 2010; Vigny et al., 2011; Koper et  
223 al., 2012; Ruiz et al., 2012; Moreno et al., 2012; Lorito et al., 2011; Lin et al., 2013; Yue et al., 2014); Iquique  
224 2014, 8.2 Mw (Ruiz et al., 2014; Hayes et al., 2014; Schurr et al., 2014; Lay et al., 2014), and Illapel 2015, 8.3  
225 Mw (Melgar et al., 2016; Heidarzadeh et al., 2016; Li et al., 2016; Lee et al., 2016; Satake and Heidarzadeh,  
226 2017). Given the large size of the Valdivia 1960 earthquake (9.5 Mw), we also include slip estimates for this  
227 event based on surface deformation data (Barrientos and Ward, 1990). The slip distribution of these events  
228 ranges from 1 meter (e.g. Tocopilla 2007, Antofagasta 1995), several meters (e.g. Illapel 2015, Iquique 2014),  
229 and more than 10 meters (Valdivia 1960, Maule 2010); however, in Figure 2, panel B, we normalize the slip

230 distribution with respect to the corresponding maximum slip in each case, plotting over the slab surface to  
231 highlight its spatial distribution. This approach aims to highlight the zones of maximum slip in each case and  
232 to appreciate their spatial and temporal distribution, under the working hypothesis that they represent the zones  
233 of maximum slip and are most likely a good proxy to identify asperities in the plate contact zone. These  
234 maximum slip zones are generally distributed between the TLF network (Figure 2).

235



236  
 237  
 238  
 239  
 240  
 241  
 242  
 243

Figure 2: Panel A: historical seismicity from the years 1450 to 2020 (for a full description of each event, see Table A.1 of the supplementary material). The lateral extent of each event indicates the NS estimate of the event name; the colour scale corresponds to the year window of each event; the  $M_w$  magnitude is represented by the width of the line. Seismo-tectonic segmentation is indicated by pink semi-transparent ribbons, which are extended downwards to the lower panels. Panel B: zones of maximum slip in the megathrust events registered at the margin of Chile since 1960, colour code represents a normalized slip to the maximum slip in each event.

244 **2.4 Cumulative seismic spatial distribution in the last 20 years**

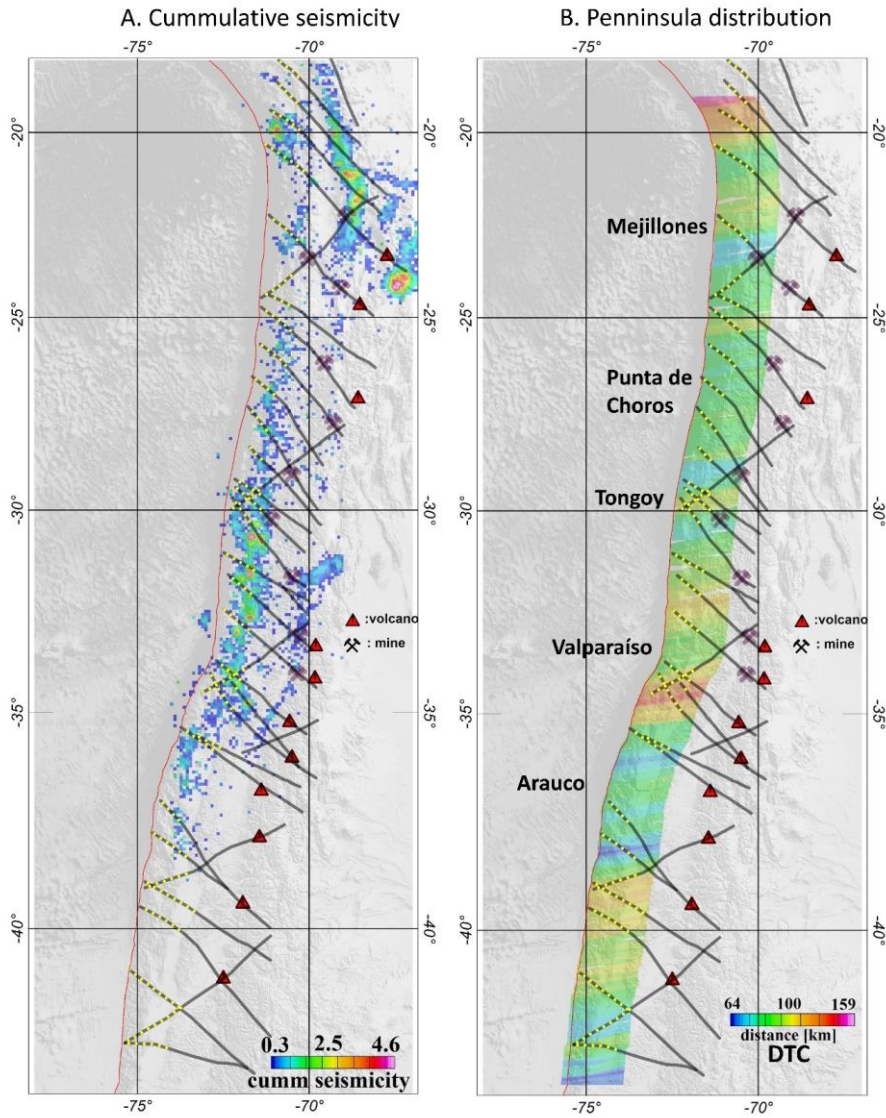
245 The seismic activity, apart from its spatiotemporal distribution around megathrust events (occasionally with  
246 foreshocks and normally with a hyperbolic distribution of aftershocks in time (Omori's law), shows some  
247 clustering (denominated in general as seismic swarms), ~~that~~ may be triggered by aseismic creep events  
248 (Forsyth et al., 2003; Roland and McGuire, 2009) associated with the presence of fluids in the fault zone. In  
249 the Andean plate convergence margin, recent studies also show examples of seismic swarm distribution  
250 attributable to fluid pore-pressure processes (e.g. Poli et al., 2017, Pasten-Araya et al., 2018). To contextualise  
251 the spatial distribution of this seismicity, we compute a normalised seismic density distribution along the  
252 margin for the last 20 years in which the seismic network is complete above magnitude 3 Mw. We exclude  
253 most of the seismicity associated with major thrust events in this period, filtering out the events at distances of  
254 less than 200 kilometres from the rupture zone in a temporal window of 200 days. We acknowledge that this  
255 20-year time window is too short to obtain a broad and complete picture of the distribution of swarms along  
256 the margin. However, as swarms normally last for just a few weeks or 1–2 months at most, the cases observed  
257 in this time window provide insights into their spatial distribution. The data used in this analysis were  
258 obtained from the database of the National Seismological Centre (CNS in Spanish). We selected data  
259 attributable to the seismogenic plate contact within a 10-kilometre-thick volume following the slab 2.0  
260 Wadati-Benioff plane (Hayes 2018). The seismic density distribution is shown in Figure 3A, panel A, we can  
261 see that seismicity tends to cluster in the vicinity of the seaward projection of the TLF.

262

263 **2.5 Distance from the trench to the shelf brake**

264 Saillard et al. (2016), show that peninsulas along subduction zones cost lines present a long-term permanent  
265 coastal uplift that can be associated with creep and aseismic slip domains. Thus, the distance from the trench  
266 to the coast (DTC) constitutes a proxy to separate seismotectonic segmentation due to the weak plate  
267 coupling. The physics behind this proposal lies in the dragging force that subduction force induces on the  
268 overriding plate, thus with less traction (weak plate coupling in the long term), the fore-arc region close to the  
269 trench should be shallower than the surroundings. To gain a broader perspective of the peninsula's  
270 distribution, Figure 3B contours the distance to the shelf brake, which is probably a better proxy for a  
271 potential uplifted domain in the coastal region. As shown in this figure, the DTC presents variations along the  
272 trench. We identify domains of short DTC associated with peninsulas in the region near to: Arauco;  
273 Valparaíso; Tongoy; Punta de Choros; and Mejillones. Based on geological and geochronological evidence in  
274 three of these peninsulas (Mejillones, Tongoy, and Arauco), Saillard et al. (2016) determined uplift rates in  
275 the range of 0.6–2 meters per thousand years in the associated terraces. These terraces have been continuously  
276 uplifting for at least the last 0.5–0.8 Myr, indicating a long-term process compared to the seismic cycle of less  
277 than 500 years. Using this evidence, in addition to the inter-seismic GPS coupling, Saillard et al. (2016) infer  
278 that these peninsula zones are associated with weak plate coupling where deformation is mostly  
279 accommodated by creep. Again, qualitatively speaking, there is a tendency to find peninsula distribution  
280 where TLF tend to concentrate in the coastal region.

281



283  
 284 **Figure 3:** Panel A: density distribution of the last 20 years of seismicity in the margin (data from National  
 285 Seismological Centre, CSN); values are normalized to better define the zones where seismicity has been  
 286 concentrated, filtering out all the aftershocks associated with major megathrust activity (Taltal 2001, Maule 2010,  
 287 Iquique 2014, and Illapel 2015). Panel B: distance from the trench to the shelf brake, projected to the convergence  
 288 direction (10E).  
 289  
 290

## 291 **2.6 Viscous coupling**

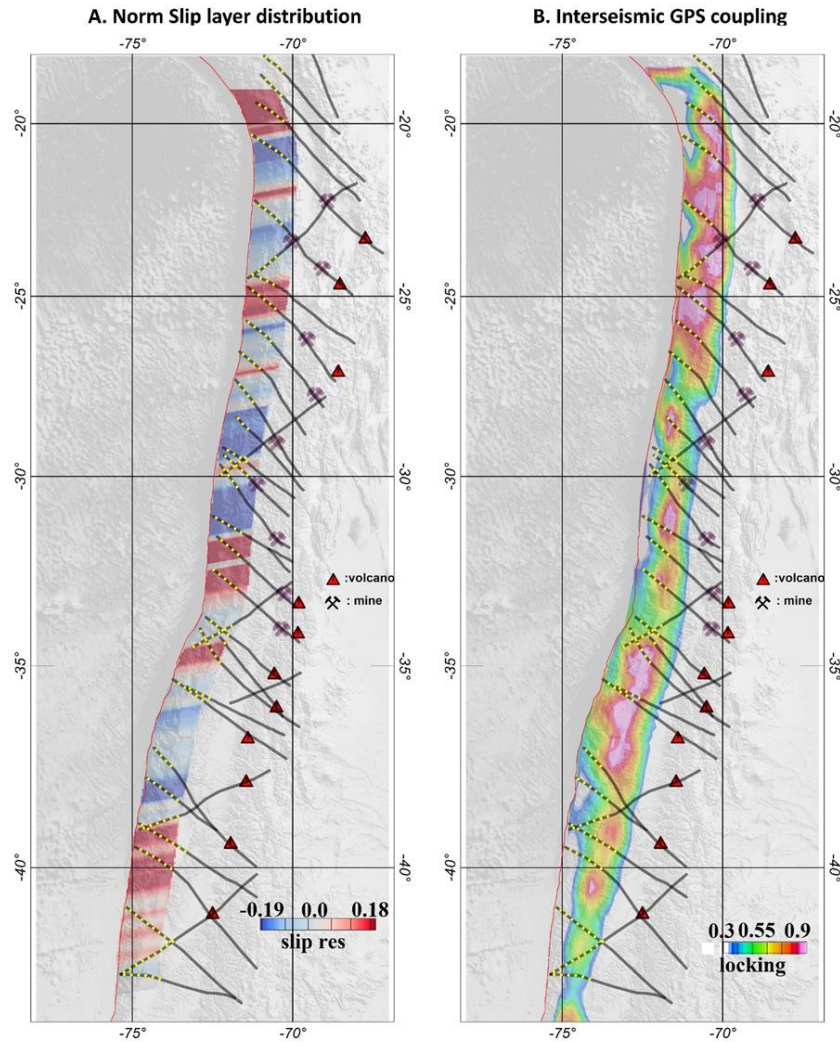
292 The negative free-air anomaly along the Chile-Perú Trench is the response to dynamic equilibrium between  
293 buoyancy and tectonic forces (Yáñez and Cembrano, 2014). The tectonic force tends to drag the continental  
294 plate downwards, whereas buoyancy restores this deformation. Assuming equilibrium between the net  
295 tectonic force and the long-term deformation (flow in continuum physics) the observed bathymetry represents  
296 this force equilibrium. Therefore, for each bathymetric observation, a given Slip Layer Viscosity (SLV)  
297 (Wdowinski, 1992) allows a match between observations and long-term viscous plate coupling. Using the  
298 methodology developed by Yáñez and Cembrano (2004), we determine the along-strike SLV in the Nazca-  
299 South America plate convergence region, considering across-strike profiles every 20 kilometres. As indicated  
300 earlier, zones of maximum slip involve wavelengths larger than 20 kilometres for the megathrust events, and  
301 therefore, a sample interval of 20 kilometres ensures appropriate along-strike resolution. In addition,  
302 following the same rationale and conclusions of Yáñez and Cembrano (2004), we estimate that the increase of  
303 the SLV in the north of the study area is due to a temperature-dependent rheology. This increase in viscous  
304 plate coupling in the north is likely to be responsible for the larger crustal shortening observed in the southern  
305 Andes in the last 20 Ma. Although other authors (e.g. Lamb and Davies 2003) consider that the deficiency in  
306 sedimentary supply in the trench in the northern Andes is the driving mechanism for the larger viscous plate  
307 coupling in the region. However, this discussion is beyond the scope of the present work, and since the  
308 viscous plate coupling correctly represents the observations we are interested here in the short-wavelength  
309 viscous plate response as a potential tool to identify zones with different degrees of coupling along the  
310 convergent margin. Therefore, we remove this regional viscous plate coupling to isolate short-wavelength  
311 features. This residual slip layer viscosity (RSLV) is included in Figure 4A (see a full discussion in  
312 Supplement A). This signal shows positive (high relative viscous plate coupling) and negative (weak relative  
313 coupling) zones. Again, we use normalized values to highlight the spatial distribution of the signal. In the  
314 supplementary material, we present a full description of the modelling used to obtain the RSLV signal. As the  
315 modelling is 1D, we extend the result of each model along the strike of the convergence (10°E).

## 316 **2.7 Inter-seismic GPS coupling**

317 GPS data provide information on the surface deformation relative to a stable continental reference. During the  
318 inter-seismic period, the slip velocity at the intraplate contact, Vinter-seismic, can be determined from a GPS  
319 network under the assumption of elastic plate deformation (e.g. Okada, 1985). This inter-seismic velocity  
320 depends on the degree of plate coupling,  $\phi$ . At maximum plate coupling ( $\phi=1$ ), Vinter-seismic is null, and at  
321 minimum plate coupling ( $\phi=0$ ), Vinter-seismic is equal to the convergence velocity ( $V_{convergence}$ ) (e.g.  
322 Nuvel1a, De Mets, et al., 1994). Or, mathematically (e.g. Metois et al., 2012),  $V_{inter-seismic}=(1-\phi)*$   
323  $V_{convergence}$ . Inter-seismic GPS coupling is presented as GPS locking data in Panel B of Figure 4 (based in  
324 a compilation of GPS information derived from different sources, Burgmann et al., 2005; Chlieh et al., 2008;  
325 Loveless & Meade, 2011; McCaffrey et al., 2002; Metois et al., 2012, 2016; Moreno et al., 2010, 2012;  
326 Wallace et al., 2004)). For the segment between Antofagasta and Copiapo (24-28°S), two new GPS plate  
327 coupling models are available (Yáñez-Cuadra et al., (2022) and González-Vidal et al., (2023)), however, we  
328 noticed that these new results share similarities do not depart significantly with the model presented in Figure

329 4b, and is therefore not necessarily thus are not included in this case. From 27°S to the north, high GPS plate  
330 coupling is generally observed, although some correspondence is observed with the local minimum and TLF  
331 distribution. Between 27°–33°S, the GPS coupling shows domains with lower values with better  
332 correspondence with TLF segmentation and the minimum in viscous coupling. To the south of 33°S, the GPS  
333 plate coupling shows a spatial distribution that again shows some coincidence with the other proxies, but also  
334 some discrepancies. This is not surprising, since GPS inter-seismic plate coupling reflects the quasi-  
335 instantaneous coupling of seismo-tectonic segments at different loading stages. Nevertheless, in most of the  
336 studied segments, the GPS plate coupling correlates relatively well with the viscous plate coupling, and the  
337 location of peninsulas and cumulative seismicity in the last 20 years.  
338





339

340 **Figure 4:** Panel A: Normalized Residual slip layer viscosity (RSLV) derived from 1D modelling along profiles  
 341 separated every 10 km and oriented along the Nazca-South American plate convergence (10°N); as this model  
 342 involves all of the slip layer, its spatial distribution is represented from the trench until 150 km landward, high  
 343 relative coupling is associated with high residual slip viscosity (see details of this computation in Supplement A) .  
 344 Panel B: GPS inter-seismic plate coupling, model 17 (Burgmann et al., 2005; Chlieh et al., 2008; Loveless &  
 345 Meade, 2011; McCaffrey et al., 2002; Metois et al., 2012, 2016; Moreno et al., 2010, 2012; Wallace et al., 2004).  
 346 Locking is restricted to the range between 0.3 to 0.9, in order to enhance the relative coupling along the plate  
 347 coupling zone.

### 348 3. Discussion

#### 349 3.1 Quantitative correlation between TLF and plate coupling proxies derived from seismicity 350 distribution, GPS and viscous coupling and coastal morphology.

351 In order to better quantify the correspondence between the spatial distribution of TLF and the indirect estimate  
352 of plate coupling described in chapter 3 we present here an objective comparison between them. This task is  
353 challenging, taking into consideration the poorly constrained data used: (a) in some cases, regional-scale  
354 geological observations (TLF and peninsula distribution); (b) different time-scale coupling estimates (inter  
355 seismic GPS locking and long term viscous coupling); (c) poorly resolved GPS solution offshore; (d) 1D  
356 modelling of viscous coupling; and (e) The lack of completeness in the seismicity record (historical record of  
357 500 years, instrumental record of megathrust events of 50 years, and cumulative seismicity of 20 years)  
358 considering a seismic cycle of a couple of hundred years in the margin. Thus, none independent proxy is capable  
359 to produce a reliable estimate by itself, but rather a combination of them. Therefore, a thorough analysis is  
360 beyond the capabilities of the data source, and what we present here, though quantitative, should be understood  
361 as a guide to determine tendencies from different and independent perspectives that as a whole, provide a more  
362 robust estimate on the link between TLF and plate coupling in the margin.

363 The approach adopted considered the spatial correlation between TLF and the six proxies described in chapter  
364 3, using the Pearson correlation coefficient between two variables ( $r_{xy}$ ) defined as:

365

$$366 r_{xy} = \frac{\sum_{i=1}^n (x_i - \bar{x})(y_i - \bar{y})}{\sqrt{\sum_{i=1}^n (x_i - \bar{x})^2 \sum_{i=1}^n (y_i - \bar{y})^2}} \quad (1)$$

367 Where  $\bar{x}$  and  $\bar{y}$  are the average value of each variable. This function  $r_{xy}$  has values between -1 (opposite  
368 correlation) to 1 (direct correlation). Values near zero mean weak or null correlation. In the application of the  
369 Pearson correlation in this case, the spatial distribution of TLF is always the  $x_i$ , and the 6 proxies used in this  
370 case are the  $y_i$  in each case. A key property of the Pearson correlation coefficient is its invariance to spatial  
371 distribution of samples and scale of the two variables. This property is particularly useful in this case where we  
372 are trying to correlate very different proxies in terms of spatial distribution and scale. The correlation is  
373 performed in moving windows bins of 32x32 km<sup>2</sup>, with an overlap of 50% between correlation estimates. The  
374 correlation is calculated in a domain of 140 km width from the trench to the east, the plate coupling zone where  
375 short-term and long-term processes take place.

376 TLF are defined as line traces, but in order to spatially correlate them with the other variables, we add  
377 a width, considering potential spatial uncertainties and zones of influence. Thus, the width of each TLF is treated  
378 as a gaussian with a value of 1 in the centre and 0 at the edge, located at 10 km from the centre, representing  
379 the deformation zone and the lateral surface covered by the potential fluid release. Such a width of 20 km seems  
380 a reasonable number for a fault system of more than 100 km length (>20%). In fact, in recorded earthquakes,  
381 like the Landers earthquake 1992 (Mw 7.3) where a rupture length of 85 km has been determined, ~~with the a~~  
382 shear deformation zone ~~of-reached~~ 12-16 km (Perrin et al., 2020). Outside the TLF domains a value of -1  
383 indicates no spatial distribution of TLF, but in practice is not relevant because the correlation is focussed inside

384 the TLF domain only. The other six proxies are treated in a different manner, depending on ~~its~~their nature. GPS  
385 plate coupling is a spatial variable covering the whole spatial range of the coupling. Looking at the GPS  
386 coupling described in Figure 4b, we can see that most of the plate contact is highly coupled, well above 0.6  
387 almost everywhere, thus in order to identify some differences in coupling we setup the mean value at 0.8. Slip  
388 viscosity layer and distance from the shelf brake to the trench are single values varying with latitude ~~which that~~  
389 are extended to spatial variables projecting the value landward following the convergence direction (~10°E). In  
390 the case of the slip coupling a mean value is already removed, thus a mean value of 0 is considered. For the  
391 shelf brake-trench distance we use the average separation of 100\_km as the mean value. Seismic cumulative  
392 density and slip distribution of megathrust events define restrictive domains along the plate coupling region.  
393 These areas are normalized between 1 and zero, and outside the region a value of -1 is assigned (no data). The  
394 same procedure is used for the boundary between historic seismicity segmentation, value 1 in the transition,  
395 and -1 outside. Since the analysis is restricted to the correlation between TLF's and the six proxies, the  
396 correlation only concerns the inner part of the TLF. Given the nature of each proxy, a low coupling at a given  
397 TLF implies a negative Pearson correlation at GPS and viscous coupling, distance from the shelf brake to the  
398 trench, and slip distribution for megathrust events (maximum slip should lie outside the TLF domain). On the  
399 contrary, positive Pearson correlation is expected with the historic segmentation and cumulative seismicity, to  
400 reflect low coupling at the TLF domain.

401 The results for each Pearson correlation coefficient spatial distribution are presented in Figure 5 in a  
402 plan view. In Figure ~~6-8~~ we present the result for the 32 relevant TLF in terms of the histogram obtained for the  
403 Pearson correlation inside the corresponding TLF domain. Over the histograms observations we include an  
404 interpretation on the correspondence with a low plate coupling condition, depending on the shape of the  
405 histogram, positive (Pearson correlation biased to the left in GPS, VISC, DIST, SLIP histograms; and biased to  
406 the right in the CUMM and HIS histograms), unclear (flat for all the proxies) and negative (Pearson correlation  
407 biased to the right in GPS, VISC, DIST, SLIP histograms; and biased to the left in the CUMM and HIS  
408 histograms) correlation. Based on this analysis we qualify the potential of each TLF in terms of its barrier  
409 potential, high, ambiguous, and poor. The criteria to establish this qualification considers the following: (a) high  
410 potential: at most one correlation is negative and by majority are positive correlation; (b) ambiguous: at most  
411 two correlations are negative and at least one correlation is positive; (c) poor: when more than three correlations  
412 are negative or none of them are positive.

413 Some relevant conclusions arise from the spatial analysis of Figure 5, 6 and 7, and histograms of Figure

414 68:

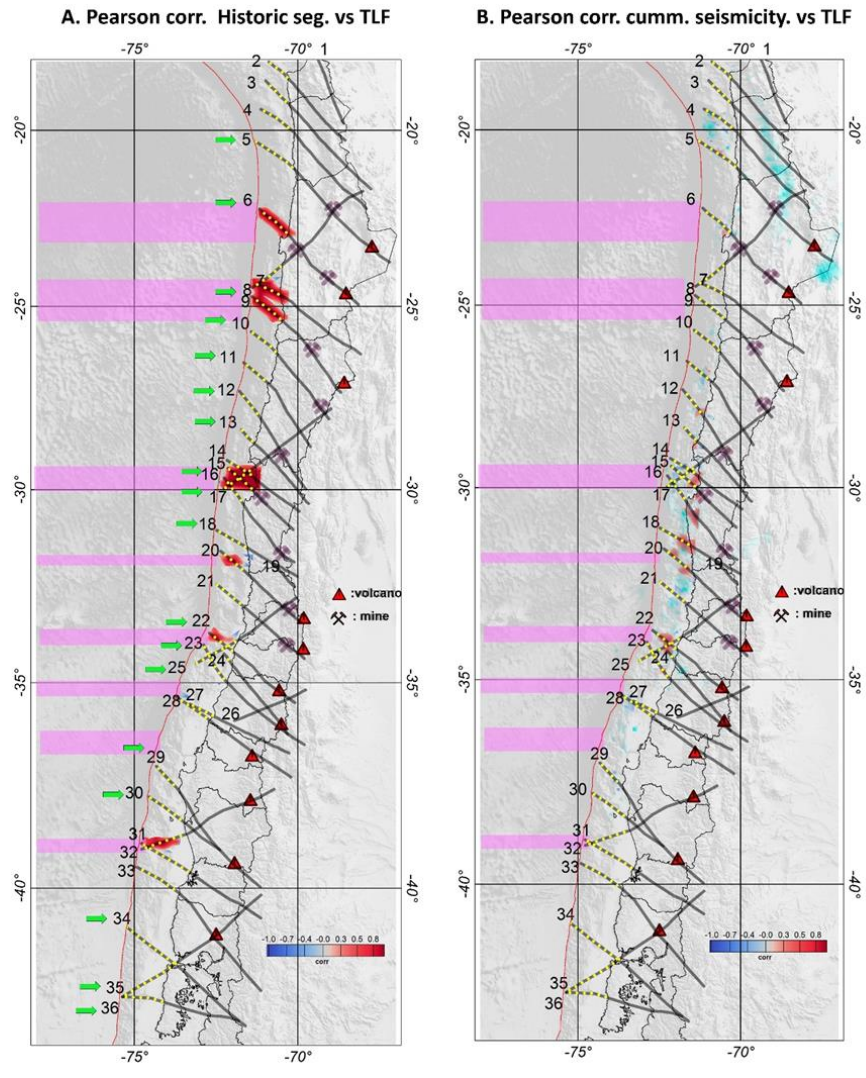
- 415 1. From the 32 relevant TLF in terms of plate coupling, 63% (20 of 32) show a high potential for a  
416 barrier behaviour, 31% (10 of 32) presents some ambiguity, and only 6% (2 of 32) TLF show a poor  
417 chance to become a barrier domain.
- 418 2. For the case of ambiguous potential, almost all of them present at least 2 positive correlation proxies.
- 419 3. For individual histograms, 54% histograms show a positive correlation, 28% are considered  
420 ambiguous, and 18% present a negative correlation.

- 421 4. Five out of seven seismotectonic boundary segments present a strong correlation with TLF spatial  
422 distribution (Figure 5a). In terms of particular histogram distribution, 11 out of 13 show a positive  
423 correlation and none of them show a negative correlation.
- 424 5. The cumulative interseismic seismicity (Figure 5a), perhaps the weakest proxy due to the lack of  
425 seismic completeness due to the very restricted time window of observation, still shows an almost  
426 100% direct correlation with the TLF traces where inter-seismic activity developed (TLF 14-15-16,  
427 TLF 18-20, TLF 22). In terms of the histogram distribution, shows a rather similar pattern, some  
428 clear positive correlation in 6 out 18 TLF and a none conclusive solution in 12 out 18 cases.
- 429 6. The spatial distribution of the slip zones of the main megathrust events recorded in the last 50 years,  
430 show a minimum positive correlation with the spatial distribution of TLF. As we can see in Figure  
431 5b6, less than 20% of the total slip domains, potential zones of asperities, correlate positively with  
432 TLF. The most conspicuous case against the rule is the slip zone of the Antofagasta 1995 that cut  
433 two TLF (7: Agua Verde-Exploradora, and 8: Antofagasta-Chonchi) and partially the Tocopilla  
434 2007 event (Mejillones-Llullaillaco TLF 6). Two complementary explanations are proposed in this  
435 case: (1) both are small events (8Mw) compared to the other megathrust events, (2) not necessarily  
436 all TLF behave as barriers all the time. For the case of Iquique 2014 event, the seaward extension of  
437 the Iquique TLF is not well constrained, and most likely run straight from landward segment, leaving  
438 the slip zone entirely to the south of TLF 4. The remaining 80% lies outside the zone of influence  
439 of TLF. In the histogram distribution, the same pattern is observed, 57% of negative Pearson  
440 correlation (or positive correlation in terms of low plate coupling), 26% of ambiguous solution and  
441 17% positive Pearson correlation. It is important to note that in several histograms of this proxy a  
442 positive correlation is adopted when a low flat response is observed, but in the left side there is a  
443 single column saturated at the maximum value for correlation -1 (most of the TLF is empty, or in  
444 other words the slip zone lies outside the TLF domain).
- 445 7. In the GPS plate coupling-TLF Pearson correlation coefficient (Figure 5b6) 50% of the cases show  
446 a negative correlation (low relative coupling), whereas 30% show some mix results, with the  
447 negative correlation concentrated in the deeper parts of the coupling, and only in 20% of the cases a  
448 positive correlation holds, mostly concentrated in the coupling zone of the Antofagasta 1995 and  
449 Tocopilla 2007 earthquakes, and probably linked with some post seismic effects. Consistently, in 18  
450 out of 32 (56%) histograms responses (Figure 68), the low coupling correlation is observed, whereas  
451 in 10 out of 32 (31%) the response is ambiguous, and the remaining 13% is associated with relatively  
452 high GPS coupling. We acknowledge that these values are very much conditioned by the choice of  
453 the threshold of 80% to separate high to low GPS coupling, but the aim is to identify less coupled  
454 domains in a signal almost saturated with high values.
- 455 8. The same type of analysis was performed for the Slip Layer viscosity – TLF Pearson correlation  
456 coefficient (Figure 5e7). In 50% of the case the correlation is opposite (low viscosity slip zones

457 corresponds with the location of TLF). In 15% of the cases, we observed mixed results, whereas in  
458 35% of the cases the correspondence is positive. Similar results are obtained with histogram  
459 responses (Figure 68), in 17 out of 32 (53%) the low coupling correlation is observed, whereas in 6  
460 out of 32 (19%) the response is ambiguous, and the remaining 28% is associated with relative high  
461 slip viscosity. One important limitation of this approach is the 1D approximation of an inherently  
462 3D process. This fact is probably the main reason for its relatively low positive response compared  
463 to the other proxies. Finally, figure 5c show the Pearson correlation coefficient for the distance from  
464 the shelf brake to the trench. In this case, the closest shelf brake to the trench at TLF intersection is  
465 a 36%, the same number of cases show an opposite behaviour and only 28% presenting mixed  
466 results. In terms of the histogram distribution (Figure 68), the same tendency is observed, but with  
467 a higher predominance of shorter distance shelf brake-trench (44%), whereas the opposite is  
468 observed in 34% of the cases and 22% show an ambiguous response. This is the proxy that show the  
469 lowest level of positiveness, probably due to the fact that other processes are also involved in the  
470 uplift of the peninsula regions, for instance the density of the crust and its relative buoyancy.

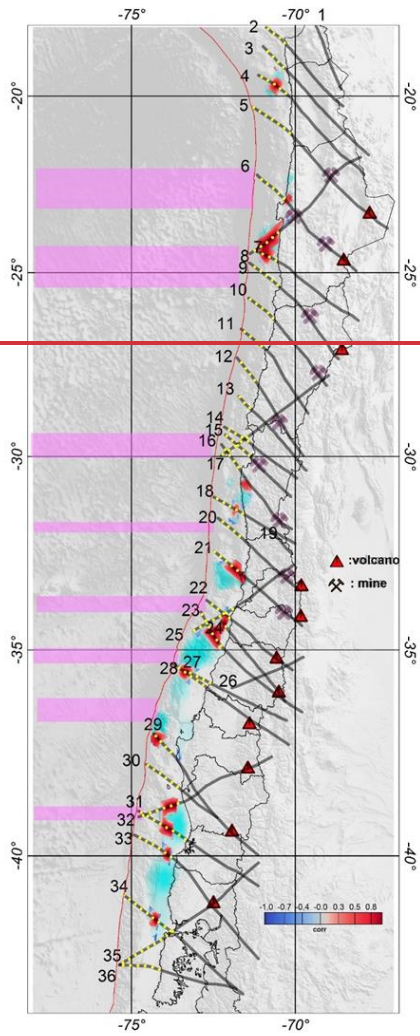
471 As we point out earlier in the text, none of the proxies by itself have the merit to account for the degree of  
472 coupling along the subduction zone, and the results emanated from the Pearson correlation demonstrate that.  
473 However, when we integrated the individual results 63% of the TLF can potentially behave as barrier, and only  
474 in two cases (6%) chances are poor. In the remaining 31% of the cases, represented as ambiguous cases, there  
475 are still some evidences of positive correlations in more than one proxy. In Figure 5a, panel A, we include a  
476 reference for the TLF with high potential to become a barrier (green arrow), and we can see that in almost all  
477 the cases they are consistent with the tectonic segmentation derived from the historic seismicity. One peculiar  
478 distribution of potentially active barrier domains is observed between 25°-30° S, the zone with less historical  
479 seismicity (Figure 2). On the other hand, not necessarily all the TLF behave as barriers, due to lack of favourable  
480 orientation, depth extent, age, dip angle, fluid content among other uncertainties. Therefore, we consider that  
481 the previous semiquantitative analysis including all the proxies, support the presence of a geological signal of  
482 low plate coupling when a TLF is present. In the next section we propose a conceptual mechanism to explain  
483 this phenomenon.

484

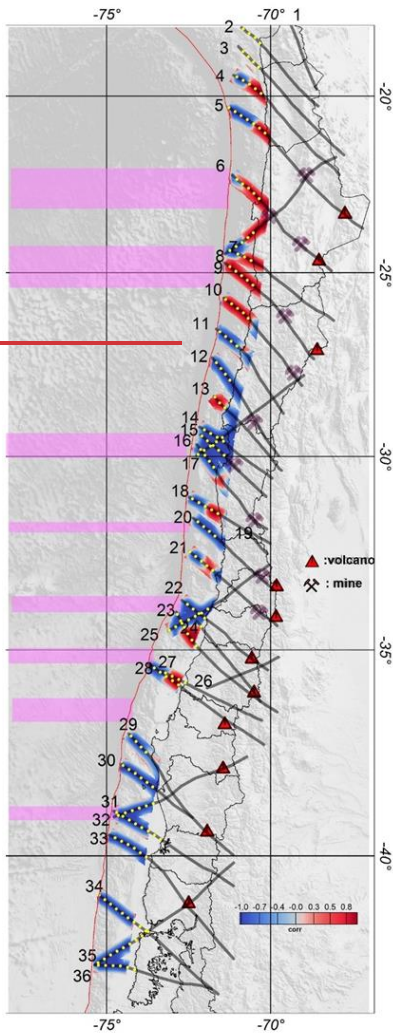


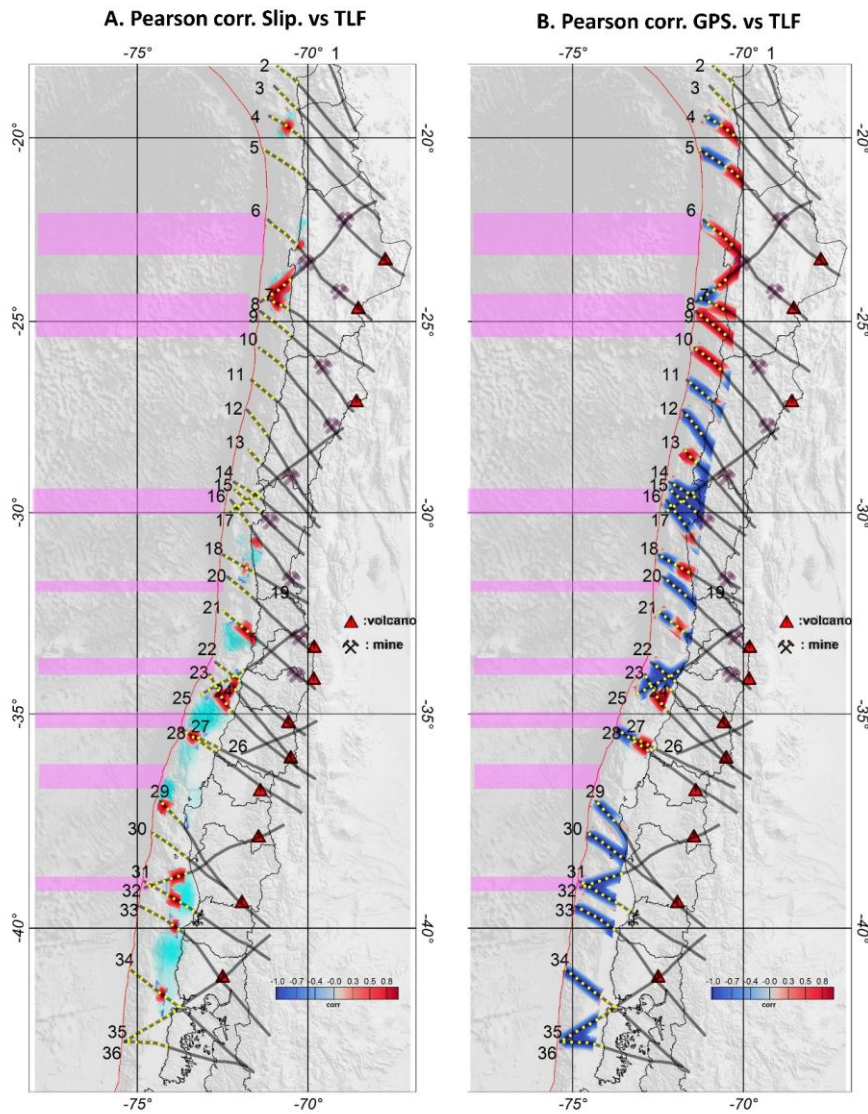
485  
 486 **Figure 5a: Pearson correlation coefficient between TLF and (A) tectonic segmentation (from Figure 2a) and (B)**  
 487 **cumulative seismicity (from Figure 3a). Colour code range from -1 (opposite correlation, blue colours) to 1 (direct**  
 488 **correlation, red colours). In panel A the green arrow shows the TLF with high potential as a barrier, according with**  
 489 **the criteria established from histograms distribution of Figure 6. Correlation is only determined in the vicinity of**  
 490 **TLF.**  
 491

C. Pearson corr. Slip. vs TLF



D. Pearson corr. GPS. vs TLF



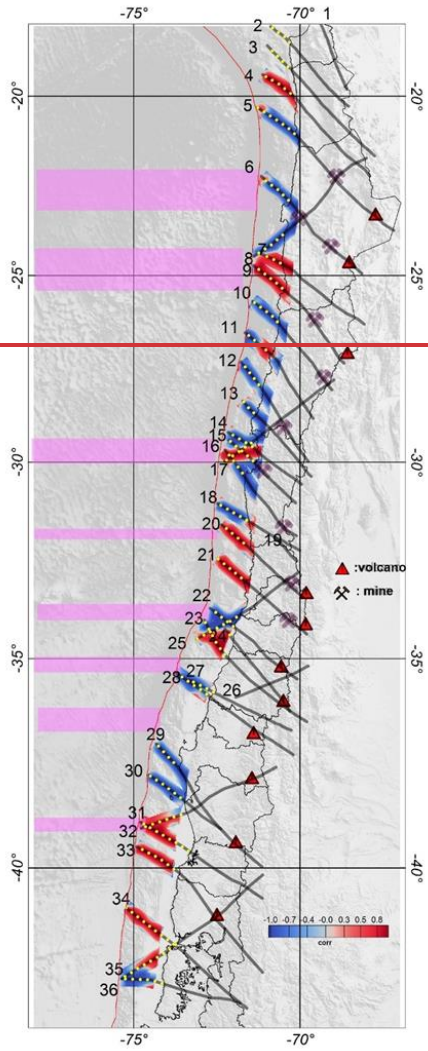


493  
 494  
 495  
 496  
 497  
 498

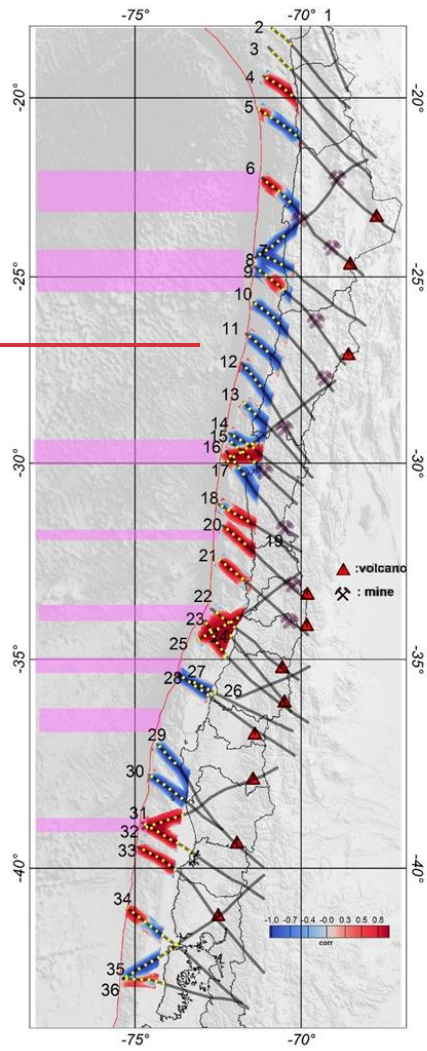
Figure 5b6: Pearson correlation coefficient between TLF and (a) normalized seismic slip (from Figure 2b) and (b) GPS coupling (from Figure 4b). Colour code range from -1 (opposite correlation, blue colours) to 1 (direct correlation, red colour). Correlation is only determined in the vicinity of TLF.

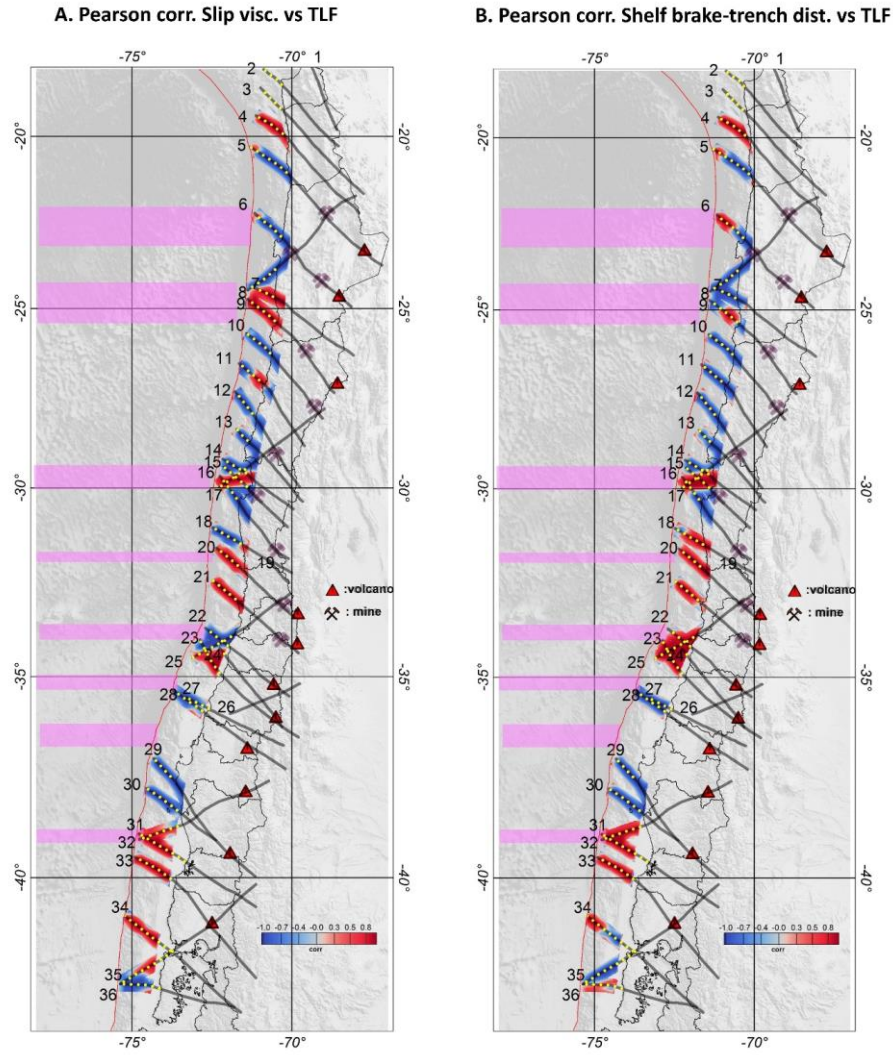


E. Pearson corr. Slip visc. vs TLF



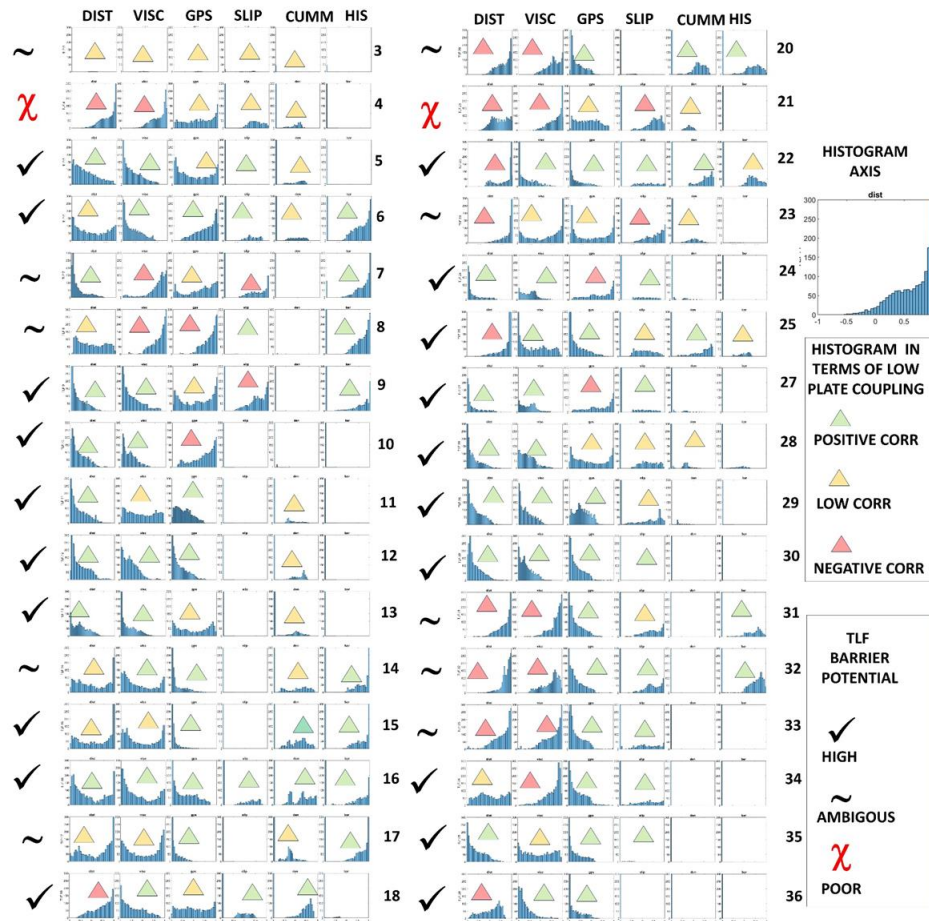
F. Pearson corr. Shelf brake-trench dist. vs TLF





500  
501  
502  
503  
504  
505  
506

Figure 5e7: Pearson correlation coefficient between TLF and tectonic slip viscosity (from Figure 4a) (eq), and distance from the trench to the shelf brake (from Figure 3b) (fb). Colour code range from -1 (opposite correlation, blue colour) to 1 (direct correlation, red colour). Correlation is only determined in the vicinity of TLF.



507  
 508  
 509  
 510  
 511  
 512  
 513  
 514

**Figure 68:** Histogram diagrams for Pearson correlation in each TLF (six histograms for each TLF). Histogram interpretation and TLF qualification as a potential barrier is indicated in inlet. TLF number is indicated to the left of each panel (a good resolution of this image is provided in the supplementary material). Correlation type is indicated by triangles in each histogram, while the estimate TLF barrier potential high to poor is indicated by symbols in the left side of each histogram.

515 **3.2 A simple conceptual barrier model: misoriented TLF as a store/released of fluids during the seismic**  
516 **cycle.**

517 Comparing the spatial distribution of the seaward extension of the TLF and the previously discussed first-order  
518 conditioning factors of the tectonic segmentation in the Andes (chapter 2), and the cross correlation described  
519 in section 4.1, we can make the following conclusions:

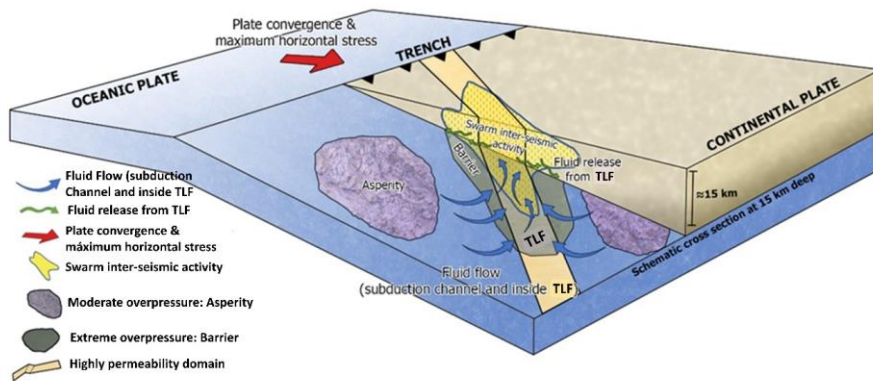
- 520 1. The coastal termination of an TLF generally occurs close to a peninsula, where the shortest trench–  
521 coast distance is observed, in spatial correspondence with zones of negative RSLV (weak viscous  
522 coupling), and in some cases also corresponding to zones of weak GPS coupling. However, it should  
523 be noted that the degrees of coupling inferred via RSLV and GPS do not map similar observation  
524 time windows, covering geological (Ma) vs seismic cycle (300–500 years) time frames, respectively.
- 525 2. During the last 60 years, slip displacements during the major megathrust earthquakes in the margin  
526 of Chile tend to be bounded by the coastal termination of an TLF in their northern and southern  
527 boundaries. Thus, if these slip zones represent a spatial distribution of asperities, the TLF correspond  
528 to zones potentially associated with barriers, consistent with the long-term low coupling inferred  
529 from RLSV, GPS plate coupling and distributions of peninsulas. the previous long-term  
530 observations.
- 531 3. Cumulative seismic activity in the last 20 years tends to nucleate in the vicinity of the seaward  
532 termination of the TLF, normally with the development of seismic swarms of 100–300 events of  
533 medium to low magnitudes during periods of several weeks at most.
- 534 4. The geological record demonstrates that TLF are long-lived structures of high permeability in  
535 comparison with the surrounding crust and most likely the underlying mantle as well, and are thus  
536 potentially efficient fluid storage structures.

537 The previous observations provide the grounds to propose a simple conceptual model to understand the role  
538 played by TLF in the tectonic segmentation of a convergent margin. These observations consistently show that  
539 TLF in the seismogenic zone are spatially correlated with long-term and short-term evidence of weak coupling  
540 behaviour. The long-term evidence involves geological processes that build up during many seismic cycles,  
541 over a time frame of millions of years, including low values of slip-layer viscosities and correspondence with  
542 the spatial distribution of peninsulas. The short-term evidence involves fragments of the seismic cycle over a  
543 time frame of less than 500 years, characterized by weak coupling zones as inferred by inter-seismic GPS  
544 observations, the flanks of slip zones of recent mega-thrust events, and the boundaries that delimit the historical  
545 record of major events. Overall, these observations consistently show that TLF domains are likely candidates  
546 for barrier zones.

547 From basic principles, the strength of a fault is controlled by the friction at the discontinuity plane. According  
548 to Amonton's law, the fault strength is proportional to the product of the normal stress and the static or dynamic  
549 friction (e.g. Scholz, 1990). In the presence of fluids, pore pressure reduces the normal stress, thereby reducing  
550 the strength of the fault (e.g. Scholz, 1990), eventually to zero if the pore pressure reaches the lithostatic pore

551 pressure. Under these supra-lithostatic fluid pressure conditions, even faults that are strongly misoriented for  
552 frictional reactivation under the prevailing stress field can be reactivated, focusing the discharge of large  
553 amounts of overpressured fluids and acting as a “fault-valve” (Sibson, 1990; Cox, 2016). Indeed, Cox (2016)  
554 showed that, under supra-lithostatic fluid pressure conditions, the typical seismic response in the faults  
555 corresponds to microseismic swarms, which, according to Sibson (2020), would concentrate at the roots of the  
556 fault system. In the case of an TLF, which is a long-lived structure transecting the whole lithosphere (e.g., Lutz  
557 et al., 2022), the root of the fault system at the Andean convergent margin corresponds to the subduction  
558 channel. Low fault strength at subduction zones can be equated to barrier zones where convergence is mostly  
559 accommodated by creep and/or micro-seismicity. The hydration of the subducting slab during its bending in the  
560 outer rise region has been widely documented in different subduction margins (e.g., Holbrook et al., 1999;  
561 Shillington et al., 2015; Contreras-Reyes et al., 2007; Moscoso and Grevemeyer, 2015; Ranero and  
562 Sallarès, 2004; Fujie et al., 2018, among others), as has the slab’s subsequent dehydration during subduction  
563 (Barriga et al., 1992; Maekawa et al., 1993; Peacock, 1993). Mantle hydrous phases (serpentinites) have also  
564 been observed in forearc regions at subduction margins (e.g. Hyndman and Peacock, 2003; Xia et al., 2015;  
565 Hansen et al., 2016), further demonstrating that subduction systems transport large amounts of water; however,  
566 the amount of water transported is still unknown (Miller et al. 2022). On the other hand, fluid flow in porous  
567 media is governed by Darcy’s law, in the opposite direction to the hydraulic head and proportional to the  
568 hydraulic permeability. Numerical models (Menant et al., 2019) have been used to determine the path of  
569 overpressured fluid flow along the subduction channel, and how strong/weak frictional channels condition the  
570 flow (weak frictional channel zones percolate more water upwards compared to strong frictional channel zones).  
571 These two domains determine the location of weak and strong coupling zones at the plate contact. Thus,  
572 according to basic principles and numerical models, water concentrates in zones of high permeability.  
573 The geological record on land shows that, in the Andean margin, TLF are associated with ore deposits  
574 clustered at the intersection of magmatic arcs that become progressively younger eastward (Piquer et al.,  
575 2016; Yáñez and Rivera, 2019; Piquer et al., 2021a; Farrar et al., 2023; Wiemer et al., 2023), covering the full  
576 tectono-magmatic history during the Mesozoic and Cenozoic. Local seismic networks deployed in Northern  
577 and Central Chile also show alignments of seismic activity along some TLF systems (Yáñez and Rivera,  
578 2019; Piquer et al., 2019, 2021a; Sielfeld et al, 2019; Pearce et al., 2021). These long- and short-term  
579 observations indicate the presence of long-lived high-permeability domains along the TLF systems in the  
580 Andean margin of Northern and Central Chile. Therefore, we postulate that TLF act as fluid sinks in the  
581 forearc region, following a continental-scale fault-valve behaviour, carrying the fluids released by slab  
582 dehydration and transported from distal locations through the subduction channel and discharging the fluids  
583 upwards and laterally through the TLF. Thus, if the proposed mechanism operates for long periods of time,  
584 the fluid distribution at the plate contact should show an uneven distribution of fluid, delimitating domains of  
585 weak and strong friction channels, which would act as seismic barriers and asperities, respectively. In this  
586 context, the spatial distribution of TLF would be associated with barriers that delimitate the tectonic  
587 segmentation. In the proposed model, tremor or swarm seismic activity represent episodic fluid release from  
588 TLF that are poorly oriented with respect to the regional tectonic stress — in this case, the NW-striking fault

589 systems oriented at a high angle relative to the ENE convergence direction. This model provides a causal link  
 590 between the presence of TLF in the upper plate and the distribution of barrier and asperity domains in the  
 591 plate interface. A schematic cartoon of this model is presented in Figure 79.  
 592 Our proposed conceptual model in which TLF's promote the development of barrier domains along the  
 593 subducting margin through the enhancement of fluid pressure complement other process at subduction zones  
 594 that also enhances the budget of localized fluids at the plate contact, among them the collision of aseismic  
 595 ridges and fracture zones, bending of the subducting plate (e.g. Ranero et al., 2008, Ranero et al., 2005,  
 596 Martinez-Loriente et al., 2019; Arai et al., 2024). In the Nazca-South America plate interaction authors had  
 597 highlighted this increase in fluids at passive ridges such as the Taltal ridge 33°S (Leon-Rios et al., 2014) and  
 598 the Juan Fernandez ridge 33.5°S (Garrido et al., 2002), and fracture zones such as the Challenger Fracture  
 599 zone 30°S (Poli et al., 2017; Maksymowicz, 2015). The volume of fluids in aseismic ridges is enhanced by  
 600 oceanic water percolation along the thicker oceanic crust, while in fracture zones as a result of the high  
 601 permeability that provides a mechanism to increase water storage prior to the subduction. These  
 602 complementary mechanisms share a common origin at the subducting plate, and in the particular case of the  
 603 Nazca plate they are oblique to the margin (roughly NE). Thus, the main difference with the proposed model  
 604 is their along strike migration with time, while in the proposed mechanism TLF belongs to the overriding  
 605 plate.



606  
 607 **Figure 79:** Schematic conceptual model of fluid transport towards TLF, following different paths in the subduction  
 608 channel, as well as upwards within the TLF. This model proposes that TLF are sink domains of slab-derived fluids  
 609 that promote the development of barrier zones and dry out the neighbouring domains where asperities develop.  
 610 Swarm clustering in spatial association with the TLF represents a mechanism for the quasi-creep release of energy  
 611 within the barrier zone.  
 612

613 **3.3 Implications**

614 If TLF act as low-friction domains (barriers) due to their capacity to store fluids released from the subducting  
615 slab and thereby dry out neighbouring zones of the subduction channel, promoting the development of a high-  
616 friction domain (asperity), we can envision a series of implications derived from the proposed model.

617 The most relevant implication is the geological control of barrier zones. This geological control exerted by high-  
618 permeability domains in the continental lithosphere (TLF) implies a spatial control of barrier zones, and thus  
619 the seismotectonic segmentation should be stable for several seismic cycles as long as the capacity of TLF to  
620 store fluids is maintained. If this scenario is correct, the estimate of the seismic risk associated with each  
621 seismotectonic segment can be assessed based on empirical fault-length laws (e.g. Anderson et al., 2016). In  
622 this context, interplate seismic swarms and slow seismic events that develop in the vicinity of TLF zones would  
623 be a mechanism for the steady release of seismic energy.

624 As discussed previously, several TLF have been identified in the Andean margin; however, little is known about  
625 their origin, width, dip, depth extent, and capacity to behave as a water sink. Therefore, further study is needed  
626 to postulate a reliable map of barrier domains in this subduction system.

627 On the other hand, seismic barriers/asperities would be conditioned by the capacity of barrier zones to  
628 mobilise and store fluids, and would thus be relatively stable in space but with a variable behaviour during  
629 several seismic cycles. If the age of the subducted slab conditions the water budget at the plate interface  
630 (Rupke et al., 2004), the progressive age increase from south to north in this margin (from 0 to 45 Ma) would  
631 be a controlling factor for the efficiency of the TLF-barrier hypothesis. Although this implication is highly  
632 speculative, the historical record shows that the largest megathrust events at the margin have occurred in  
633 Southern Chile, including the 9.3Mw 1960 Valdivia Earthquake, the largest event recorded worldwide.

634

#### 635 4. Conclusions

636 Based on first order geological and geophysical observations of the Nazca-South America plate convergence  
637 we propose a conceptual model to understand the tectonic segmentation in the Andean region.

638 Observations include historical seismicity and the associated seismotectonic segmentation. Major thrust events  
639 occurred in the region in the last 60 years, defining domains of asperities. GPS and viscous plate coupling that  
640 provide independent proxies to establish potential domains of barriers (low plate coupling) and asperities (high  
641 plate coupling). Location of low plate coupling domains is further associated with the spatial distribution of  
642 peninsulas (less basal erosion) and cumulative seismicity during the inter-seismic period (slow interplate  
643 seismic events, creeping, associated with fluid release).

644 Key element in the model is played by trans-lithospheric faults (TLF). Landward, this TLF system concentrate  
645 the occurrence of major hydrothermal ore deposits and some active volcanism, denoting their intrinsic high  
646 permeability. Thus, at their seaward edge the TLF domains act as sink and release of fluids during the seismic  
647 cycle. The fluid is captured from the slab through the subducting channel, and continuously release to the plate  
648 contact, promoting the growth of barriers beneath them (excess of fluids), and asperities laterally (reduction in  
649 fluid content).

650 If the interaction of first order continental structures and the fluid content of the subducting slab plays a  
651 central role in the seismotectonic segmentation of convergence zones, a carefully understanding of the

652 overriding plate geology and associated structures could be instrumental to better understand the associated  
653 seismic risk.

654

655 **Competing interests:** The contact author has declared that none of the authors has any competing interests.

656 **Acknowledge:** This research was partially supported by Fondef project D10I1027. J.P. acknowledges support  
657 from ANID-FONDECYT grant 11181048 and Amira Global P1249 project. We also would like to thanks Prof.

658 Booth-Rea and one anonymous reviewer for their valuable observations. We think the paper has been [greatly](#)  
659 improved with the observations made by both reviewers.

660 **Data Availability Statement:** The data used in this paper is derived from published papers, indicated in the  
661 text, and topographic/bathymetric data extracted from public source, ETOPO 2022. DOI: 10.25921/fd45-gt74.



## References

- 665 Aki, K., (1984). Asperities, barriers, characteristic earthquakes and strong motion prediction. *Journal of Geophysical Research* 89: doi: 10.1029/JB089iB07p05867, 1984-Issn: 0148-0227.
- Angermann, D., J. Klotz, C. Reigber, (1999). Space-geodetic estimation of the Nazca–South America Euler vector. *Earth and Planetary Science Letters*, 171(3), 329–334. [https://doi.org/10.1016/S0012-821X\(99\)00173-9](https://doi.org/10.1016/S0012-821X(99)00173-9), 1999.
- Arai, R., Shiraishi, K., Nakamura, Y. et al., Thick slab crust with rough basement weakens interplate coupling in the western Nankai Trough. *Earth Planets Space* 76, 73, (2024). <https://doi.org/10.1186/s40623-024-02025-4>, 2024.
- 670 Arriagada, C., P. Roperch, C. Mpodozis, G. Dupont-Nivet, P. R. Cobbold, A. Chauvin, J. Cortés, (2003). Paleogene clockwise tectonic rotations in the forearc of central Andes, Antofagasta region, northern Chile. *Journal of Geophysical Research: Solid Earth*, 108(B1), 2003.
- Aron, F., R. Allmendinger, J. Cembrano, G. González, and G. Yáñez, (2013). Permanent Forearc Extension and Seismic Segmentation: Insights from the 2010 Maule Earthquake, Chile, *J. Geophys. Res.*, doi:10.1029/2012JB009339, 2013.
- 675 Avouac, J.P., (2007). Dynamic Processes in Extensional and Compressional Settings - Mountain Building: From Earthquakes to Geological Deformation, *Treatise on Geophysics*, 6, 377 – 439, 2007.
- Barrientos S.E., S.N. Ward, S.N., (1990). The 1960 Chile earthquake: inversion for slip distribution from surface deformation, *Geophysical Journal International*, Volume 103, Issue 3, Pages 589–598, <https://doi.org/10.1111/j.1365-246X.1990.tb05673.x>, 1990.
- 680 Barriga, F. J. A. S., W.S. Fyfe, W.S., L.A. LANDEFELD, Landefeld, L.A., A. Ribeiro, A., (1992). Mantle eduction: Tectonic fluidisation at depth. *Earth Science Reviews* 32, 123-9, 1992.
- Bilek, S. L., S.Y. Schwartz, H.R. DeShon, (2003). Control of seafloor roughness on earthquake rupture behavior. *Geology* 31, 455–458
- W. F. Brace, J. D. Byerlee, J.D. —, Stick-Slip as a Mechanism for Earthquakes. *Science* 153, 990 - 992, (1966). DOI:10.1126/science.153.3739.990, 1966.
- 685 R. Burridge, R., L. Knopoff, L., Model and theoretical seismicity. *Bulletin of the Seismological Society of America* 1967; 57 (3): 341–371. doi: <https://doi.org/10.1785/BSSA0570030341>, 1967.
- Bürgmann, R., Kogan, M. G., Steblov, G. M., Hilley, G., Levin, V. E., & Apel, E., (2005). Interseismic coupling and asperity distribution along the Kamchatka subduction zone. *Journal of Geophysical Research*, 110, B07405. <https://doi.org/10.1029/2005JB003648>, 2005.
- 690 Cahill, T., and B.L. Isacks, B.L., (1992). Seismicity and shape of the subducted Nazca Plate, *Journal of Geophysical Research*, vol 97, B12, 17503-17529, 1992.

Con formato: Inglés (India)

Con formato: Inglés (India)

Con formato: Inglés (India)

695 ~~Calle-Gardella, D., Comte, D., Fariás, M. et al., Three-dimensional local earthquake tomography of pre-Cenozoic structures in the coastal margin of central Chile: Pichilemu fault system. J Seismol 25, 521–533 (2021).~~ <https://doi.org/10.1007/s10950-021-09989-w>, 2021.

Carretier, S., Regard, V., Vassallo, R., Aguilar, G., Martinod, J., Riquelme, R., ... & Lagane, C. ~~(2013)~~. Slope and climate variability control of erosion in the Andes of central Chile. *Geology*, 41(2), 195-198, 2013.

Cembrano, J., and L. Lara, L., ~~(2009)~~. The link between volcanism and tectonics in the southern volcanic zone of the Chilean Andes: A review, *Tectonophysics* 471, 96–113, 2009.

700 Chernicoff, C.J., J.P. Richards, J.P., E.O. Zappettini, E.O., ~~(2002)~~. Crustal lineament control on magmatism and mineralization in northwestern Argentina: geological, geophysical, and remote sensing evidence. *Ore Geology Reviews* 21, 127-155, 2002.

Chlieh, M., J.-B. De Chabaliér, J. B., J.-C. Ruegg, J. C., R. Armijo, R., R. Dmowska, R., J. Campos, J. K., L. Feigl, K. L., ~~(2004)~~. Crustal deformation and fault slip during the seismic cycle in the North Chile subduction zone, from GPS and InSAR observations, *Geophysical Journal International* Volume 158, Issue 2 p. 695-711, 2004.

705 Chlieh, M., Avouac, J. P., Sieh, K., Natawidjaja, D. H., & Galetzka, J., ~~(2008)~~. Heterogeneous coupling of the Sumatran megathrust constrained by geodetic and paleogeodetic measurements. *Journal of Geophysical Research*, 113, B05305. <https://doi.org/10.1029/2007JB004981>, 2008.

~~Comte, D., A. Eisenberg, A., E. Lorca, E., M. Pardo, M., L. Ponce, L., R. Saragoni, R., S. K. Singh, S. K., G. Suárez, G., (1986)~~. The 1985 Central Chile Earthquake: A Repeat of Previous Great Earthquakes in the Region?, *Science*, 07-25 233(4762): 449-453, 1986.

710 Contreras-Reyes, E., I. Grevemeyer, I., E. R. Flueh, E. R., M. Scherwath, M., and M. Heesemann, M., ~~(2007)~~. Alteration of the subducting oceanic lithosphere at the southern central Chile trench–outer rise, *Geochem. Geophys. Geosyst.*, 8, Q07003, doi:10.1029/2007GC001632, 2007.

Cox, S.F., ~~(2016)~~. Injection-driven swarm seismicity and permeability enhancement: implications for the dynamics of hydrothermal ore systems in high fluid-flux, overpressured faulting regimes. *Economic Geology* 111, pp. 559–587, 2016.

715 Creixell, C., Parada, M. A., Morata, D., Vázquez, P., Pérez de Arce, C., Arriagada, C., ~~(2011)~~. Middle-Late Jurassic to Early Cretaceous transtension and transpression during arc building in Central Chile: evidence from mafic dike swarms, *Andean Geol.* 38, 37-63, 2011.

~~B. Delouis, B., T. Monfret, T., L. Dorbath, L., M. Pardo, M., L. Rivera, L., D. Comte, D., H. Haessler, H., J.P. Caminade, J.P., L. Ponce, L., E. Kausel, E., A. Cisternas, A., (1997)~~. The Mw = 8.0 Antofagasta (northern Chile) earthquake of 30 July 1995: A precursor to the end of the large 1877 gap. *Bulletin of the Seismological Society of America*, 87 (2): 427–445. doi: <https://doi.org/10.1785/BSSA0870020427>, 1997.

720 ~~Delouis, B., J.M. Nocquet, J.M., M. Vallée, M., (2010)~~. Slip distribution of the February 27, 2010 Mw = 8.8 Maule Earthquake, central Chile, from static and high-rate GPS, InSAR, and broadband teleseismic data, *Geophys. Res. Lett.*, 37, L17305, doi:10.1029/2010GL043899, 2010.

725

Con formato: Inglés (India)

Con formato: Inglés (India)

Con formato: Inglés (India)

Con formato: Español (Chile)

Con formato: Español (Chile)

Con formato: Inglés (India)

Con formato: Inglés (India)

Con formato: Inglés (India)

Con formato: Inglés (India)

Con formato: Italiano (Suiza)

Con formato: Italiano (Suiza)

Con formato: Inglés (India)

Con formato: Inglés (India)

Con formato: Inglés (India)

Con formato: Inglés (India)

Con formato: Inglés (India)

Con formato: Inglés (India)

Con formato: Inglés (India)

Con formato: Inglés (India)

Con formato: Inglés (India)

Con formato: Inglés (India)

Con formato: Inglés (India)

Con formato: Inglés (India)

Con formato: Inglés (India)

- Demets, C., ~~R. Gordon, D. Argus, S. Stein, (1990)~~. Current Plate Motions. *Geophysical Journal International*. 101–425 - 478. 10.1111/j.1365-246X.1990.tb06579.x. 1990.
- Espinoza, M., Montecino, D., Oliveros, V., Astudillo, N., Vásquez, P., Reyes, R., Celis, C., González, R., Contreras, J., Creixell, C., Martínez, A., ~~(2019)~~. The synrift phase of the early Domeyko Basin (Triassic, northern Chile): Sedimentary, volcanic, and tectonic interplay in the evolution of an ancient subduction-related rift basin. *Basin Research* 31, 4-32. 2019.
- 730 ~~Farías M., D. Comte, S. Roecker, D. Carrizo, M. Pardo, (2011)~~. Crustal extensional faulting triggered by the 2010 Chilean Earthquake: The Pichilemu Seismic Sequence: *Tectonics*, v. 30, TC6010, doi:10.1029/2011TC002888. 2011.
- Farrar, A.D., Cooke, D.R., Hronsky, J.M.A., Wood, D.G., Benavides, S., Cracknell, M.J., Banyard, J.F., Gigola, S., Ireland, T., Jones, S.M., Piquer, J., ~~(2023)~~. A Model for the lithospheric architecture of the Central Andes and the localization of giant porphyry copper deposit clusters. *Economic Geology* 118 (6), 1235–1259, doi: 10.5382/econgeo.5010. 2023.
- 735 Fedotov, S. A., ~~(1968)~~. On seismic cycle, possibility of quantitative seismic regionalization and long-term seismic prediction. In *Seismic Zoning of the USSR* (ed. S. Medvedev) (Nauka, Moscow) pp. 121-150. 1968.
- Fischer, T., ~~(2021)~~. Control estructural sobre la circulación de magmas y fluidos hidrotermales Miocenos y Cuaternarios en el sector de La Invernada, Región del Maule, Chile. *Valdivia: Universidad Austral de Chile*, 314. 2021.
- 740 Forsyth, D., ~~W. Yang, M.D. Mangriotis, Y. Shen, (2003)~~. Coupled seismic slip on adjacent oceanic transform faults. *Geophysical Research Letters*, 30(12). 2003.
- Fujie, G., ~~S. Kodaira, Y. Kaiho, et al., (2018)~~. Controlling factor of incoming plate hydration at the north-western Pacific margin. *Nat Commun* 9, 3844. 2018.
- Gana, P., ~~R. Wall, A. Gutiérrez, (1996)~~. Mapa Geológico del Área de Valparaíso – Cuarcaví. *Regiones de Valparaíso y Metropolitana, Mapas Geológicos N°1, Escala 1:100.000. Servicio Nacional de Geología y Minería, Chile*. 1996.
- 745 Garrido, I., ~~J. Cembrano, A. Siña, P. Stedman, G. Yáñez, (2002)~~. High magma oxidation state and contractional deformation: key factors in the generation of Andean porphyry copper deposits, Central Chile (31–34°S). *Revista Geológica de Chile*, Vol. 29, No. 1, p. 3-14. 2002.
- ~~Geersen, J., C. Ranero, U. Barckhausen, U., (2015)~~. Subducting seamounts control intraplate coupling and seismic rupture in the 2014 Iquique earthquake area. *Nat Commun* 6, 8267. <https://doi.org/10.1038/ncomms9267>. 2015.
- 750 Giambiagi, L., Álvarez, P., Creixell, C., Mardonez, D., Murillo, I., Velásquez, R., Lossada, A., Suriano, J., Mescua, J., Barrionuevo, M., ~~(2017)~~. Cenozoic Shift From Compression to Strike-Slip Stress Regime in the High Andes at 30°S, During the Shallowing of the Slab: Implications for the El Indio/Tambo Mineral District. *Tectonics*, Vol. 36, Issue 11. <https://doi.org/10.1002/2017TC004608>. 2017.
- 755 Glodny, J., ~~H. Echter, S. Collao, M. Ardiles, P. Burón, O. Figueroa, (2008)~~. Differential Late Paleozoic active margin evolution in South-Central Chile (37°S-40°S) -The Lanahue Fault Zone. *Journal of South American Earth Sciences*, 26, 4, 397-411 DOI: 10.1016/j.jsames.2008.06.001. 2008.
- Gutscher, M.A., ~~J. Malavielle, S. Lallemand, J.Y. Collot, J.Y., (1999)~~. Tectonic segmentation of the north Andean margin: impact of the Carnegie Ridge collision, *Earth and Planetary Science Letters*, 168, 255-270. 1999.

Con formato: Inglés (India)

Con formato: Inglés (India)

Con formato: Inglés (India)

Con formato: Inglés (India)

Con formato: Inglés (India)

Con formato: Inglés (India)

Con formato: Inglés (India)

Con formato: Inglés (India)

Con formato: Inglés (India)

Con formato: Inglés (India)

Con formato: Español (Chile)

Con formato: Español (Chile)

Con formato: Inglés (India)

Con formato: Inglés (India)

Con formato: Inglés (India)

Código de campo cambiado

Con formato: Inglés (India)

- 760 ~~González-Vidal, D., Moreno, M., Sippl, C., Baez, J. C., Ortega-Culaciati, F., Lange, D., et al. (2023).~~ Relation between oceanic plate structure, patterns of interplate locking and microseismicity in the 1922 Atacama seismic gap. *Geophysical Research Letters*, 50, e2023GL103565. <https://doi.org/10.1029/2023GL103565>, 2013.
- Haberland, C., ~~A. Rietbrock, A., D. Lange, D., K. Bataille, K., S. Hofmann, S., (2006).~~ Interaction between forearc and oceanic plate at the south-central Chilean margin as seen in local seismic data. *Geophysical Research Letters* 33: 1-5, 2006.
- 765 Hansen, S., ~~B. Schmandt, B., A. Levander, A., et al., (2016).~~ Seismic evidence for a cold serpentinized mantle wedge beneath Mount St Helens. *Nat Commun* 7, 13242. <https://doi.org/10.1038/ncomms13242>, 2016.
- Hayes, G., ~~(2018).~~ Slab2 – A Comprehensive Subduction Zone Geometry Model: U.S. Geological Survey data release, <https://doi.org/10.5066/F7PV6JNV>, 2018.
- Hayes, G., ~~M. Herman, M., W. Barnhart, W., et al., (2014).~~ Continuing megathrust earthquake potential in Chile after the 2014 Iquique earthquake. *Nature* 512, 295–298. <https://doi.org/10.1038/nature13677>, 2014.
- 770 Heidarzadeh, M., Murotani, S., Satake, K., Ishibe, T., Gusman, A.R., ~~(2016).~~ Source model of the 16 September 2015 Illapel, Chile Mw 8.4 earthquake based on teleseismic and tsunami data. *Geophys. Res. Lett.* 43, 643–650, 2016.
- Hyndman, R.D., ~~S. M. Peacock, S.M., (2002).~~ Serpentinization of the forearc mantle, *Earth and Planetary Science Letters* 212, 417-432, 2002.
- 775 Kay, S.M., Mpodozis, C., ~~(2002).~~ Magmatism as a probe to the Neogene shallowing of the Nazca plate beneath the modern Chilean flat slab. *Journal of South American Earth Sciences* 15, 39-57, 2002.
- Kimura, G., ~~A. Yamaguchi, A., M. Masataka, M., (2018).~~ Upper-plate tectonic hysteresis and segmentation of the rupture area during seismogenesis in subduction zones—A case study of the Nankai “rough”, *Geology and Tectonics of Subduction Zones: A Tribute to Gaku Kimura, Timothy Byrne, Michael B. Underwood, III, Donald Fisher, Lisa McNeill, Demian Saffer, Kohtar Ujii, Asuka Yamaguchi*, [https://doi.org/10.1130/2018.2534\(05\)](https://doi.org/10.1130/2018.2534(05)), 2018.
- 780 ~~J. Kley, J., C.R. Monaldi, C.R., J.A. Salfity, J.A., (1999).~~ Along-strike segmentation of the Andean foreland: causes and consequences, *Tectonophysics*, Volume 301, Issues 1–2, Pages 75-94, ISSN 0040-1951, [https://doi.org/10.1016/S0040-1951\(98\)90223-2](https://doi.org/10.1016/S0040-1951(98)90223-2), 1999.
- Kohler, P. A., ~~(2016).~~ Geología ~~36~~ del Complejo Volcánico Laguna del Maule y su control sobre la deformación cortical, ~~36~~ Undergraduate thesis. Concepción: Universidad de Concepción, 225, 2016.
- 785 ~~Koper, K. D., A. R. Hutko, A.R., T. Lay, T., and O. Sufri, O., (2012).~~ Imaging short-period seismic radiation from the 27 February 2010 Chile (Mw 8.8) earthquake by back-projection of P, PP, and PKIKP waves, *J. Geophys. Res.* 117, B02308, 2012.
- Lamb, S. ~~and P., Davis, P., (2003).~~ Cenozoic climate change as a possible cause for the rise of the Andes. *Nature*. 425. 792-7. [10.1038/nature02049](https://doi.org/10.1038/nature02049), 2003.
- 790 Lanza, F., ~~A. Tibaldi, A., F.L. Bonali, F.L., C. Corazzato, C., (2013).~~ Space-time variations of stresses in the Miocene–Quaternary along the Calama–Olacapato–El Toro Fault Zone, Central Andes. *Tectonophysics* 593, 33-56, 2013.

Con formato: Inglés (India)

Con formato: Inglés (India)

Con formato: Inglés (India)

Con formato: Inglés (India)

Con formato: Inglés (India)

Con formato: Inglés (India)

Con formato: Inglés (India)

Con formato: Inglés (India)

Con formato: Italiano (Suiza)

- Lara, L., ~~A.~~-Lavenu, ~~A.~~, ~~J.~~-Cembrano, ~~J.~~, ~~C.~~-Rodríguez, ~~C.~~, ~~(2006)~~. Structural controls of volcanism in transversal chains: resheared faults and neotectonics in the Cordón Caulle–Puyehue area (40.5°S), Southern Andes. *Journal of Volcanology and Geothermal Research* 158, 70–86. <https://doi.org/10.1016/j.jvolgeores.2006.04.017>, 2006.
- 795 Lay, T., ~~H.~~-Kanamori, ~~H.~~, and ~~L.~~-Ruff, ~~L.~~, ~~(1982)~~. The asperity model and the nature of large subduction zone earthquake occurrence, *Earthquake Prediction Research*, 1, 3-71, 1982.
- Lay, T., and ~~S. L.~~-Bilek, ~~S. L.~~, ~~(2007)~~. Anomalous earthquake ruptures at shallow depths on subduction zone megathrusts, in: *The Seismogenic Zone of Subduction Thrust Faults*, Edited by T. H. Dixon and J. C. Moore, Columbia University Press, New York, pp. 476-511, 2007.
- 800 Lay, T., ~~C. J.~~-Ammon, ~~J.~~, ~~H.~~-Kanamori, ~~H.~~, ~~K. D.~~-Koper, ~~K. D.~~, ~~O.~~-Sufri, ~~O.~~, and ~~A. R.~~-Hutko, ~~A. R.~~, ~~(2010)~~. Teleseismic inversion for rupture process of the 27 February 2010 Chile (Mw 8.8) earthquake, *Geophys. Res. Lett.*, 37, L13301, doi:10.1029/2010GL043379, 2010.
- Lay, T., ~~H. E. E.~~-Yue, ~~H. E. E.~~, ~~E. E.~~-Brodsky, ~~E. E.~~, and ~~C.~~-An, ~~C.~~, ~~(2014)~~. The 1 April 2014 Iquique, Chile Mw 8.1 earthquake rupture sequence, *Geophys. Res. Lett.*, 41, doi:10.1002/2014GL060238, 2014.
- 805 Lay, T., ~~(2015)~~. The surge of great earthquakes from 2004 to 2014, *Earth and Planetary Sci. Lett.*, Invited Frontiers Paper, 409, 133-146, 2015.
- Lee, S.J., ~~T. Y.~~-Yeh, ~~T. Y.~~, ~~T. C.~~-Lin, ~~T. C.~~, ~~Y. Y.~~-Lin, ~~Y. Y.~~, ~~T. R.~~-Song, ~~T. R.~~, ~~B. S.~~-Huang, ~~B. S.~~, ~~(2016)~~. Two-stage composite megathrust rupture of the 2015 Mw8.4 Illapel, Chile, earthquake identified by spectral-element inversion of teleseismic waves, *Geophys. Res. Lett.*, 43, 4979– 4985, doi:10.1002/2016GL068843, 2016.
- 810 Leon-Rios, S., Reyes-Wagner, V., Calle-Gardella, D., Rietbrock, A., Roecker, S., Maksymowicz, A., & Comte, D., ~~(2024)~~. Structural characterization of the Taltal segment in northern Chile between 22°S and 26°S using local earthquake tomography. *Geochemistry, Geophysics, Geosystems*, 25, e2023GC011197. <https://doi.org/10.1029/2023GC011197>, 2024.
- Li, L., T. Lay, ~~K. F.~~-Cheung, ~~K. F.~~, and ~~L.~~-Ye, ~~L.~~, ~~(2016)~~. Odellingdeling of teleseismic and tsunami wave observations to constrain the 16 September 2015 Illapel, Chile, MW 8.3 earthquake rupture process, *Geophysical Research Letters*, 43, 4303-4312, doi:10.1002/2016GL068674, 2016.
- 815 Lin, Y. N. N., ~~A.~~-Sladen, ~~A.~~, ~~F.~~-Ortega-Culaciati, ~~F.~~, ~~F. M.~~-Simons, ~~M.~~, ~~J. P.~~-Avouac, ~~J. P.~~, ~~E. J.~~-Fielding, ~~E. J.~~, ~~A.~~-Socquet, ~~A.~~, ~~(2013)~~. Coseismic and postseismic slip associated with the 2010 Maule Earthquake, Chile: Characterizing the Arauco Peninsula barrier effect. *Journal of Geophysical Research: Solid Earth*, 118(6), 3142-3159, 2013.
- 820 Lorito, S., ~~F.~~-Romano, ~~F.~~, ~~S.~~-Atzori, ~~S.~~, et al., ~~(2011)~~. Limited overlap between the seismic gap and coseismic slip of the great 2010 Chile earthquake. *Nature Geosci* 4, 173–177 <https://doi.org/10.1038/ngeo1073>, 2011.
- Loveless, J. P., & Meade, B. J. ~~(2011)~~. Stress modulation on the San Andreas fault by interseismic fault system interactions. *Geology*, 39, 1035–1038. <https://doi.org/10.1130/G32215.1>, 2011.
- 825 Lutz, B.M., Axen, G.J., van Wijk, J.W., Phillips, F.M., ~~(2022)~~. Whole-lithosphere shear during oblique rifting. *Geology* 50, 412–416, <https://doi.org/10.1130/G49603.1>, 2022.

Con formato: Inglés (India)

Con formato: Italiano (Suiza)

Código de campo cambiado

Con formato: Inglés (India)

- Maekawa H., ~~M. Shzui, M., T. Ishii, T., P. Freyer P., J.A. Pearce J.A., (1993).~~ Blueshist metamorphism in active subduction zone, *Nature*, v. 364, p. 520-523, [1993](#).
- Maksymowicz A., ~~(2015).~~ The geometry of the Chilean continental wedge: Tectonic segmentation of subduction processes off Chile, *Tectonophysics Volume 659*, 30 September 2015, Pages 183-196, <https://doi.org/10.1016/j.tecto.2015.08.007>, [2015](#).
- 830 Martínez-Loriente, S., Sallarès, V., R. Ranero, C., B. Ruh, J., Barckhausen, U., Grevemeyer, I., & Bangs, N. ~~(2019).~~ Influence of incoming plate relief on overriding plate deformation and earthquake nucleation: Cocos Ridge subduction (Costa Rica). *Tectonics*, 38, 4360–4377. <https://doi.org/10.1029/2019TC005586>, [2019](#).
- Marrett, R.A., ~~R.W. Allmendinger, R.W., R.N. Alonso, R.N., R.E. Drake, R.E. (1994).~~ Late Cenozoic tectonic evolution of the Puna Plateau and adjacent foreland, northwestern Argentine Andes. *Journal of South American Earth Sciences*, Vol. 7, N°2, pp179-207, [1994](#).
- 835 Mccaffrey, R., Stein, S., & Freymueller, J. ~~(2002).~~ Crustal block rotations and plate coupling. *Geodynamics Series*, **30**, 101–122, [2002](#).
- McCuaig, T.C., Hronsky, J.M.A., ~~(2014).~~ The mineral system concept: the key to exploration targeting. *Society of Economic Geologists, Special Publication 18*, 153-176, [2014](#).
- 840 Melgar, D., ~~W. Fan, W., S. Riquelme, S. J. Gengm, J., C. Liang, C., M. Fuentes, M., G. Vargas, G., R. M. Allen, R. M., P. M. Shearer, P. M., and E. J. Fielding, E. J. (2016).~~ Slip segmentation and slow rupture to the trench during the 2015, Mw8.3 Illapel, Chile earthquake, *Geophys. Res. Lett.*, 43, 961–966, doi:10.1002/2015GL067369, [2016](#).
- Melnick, D., ~~H.P. Echter, H.P., (2006).~~ Morphotectonic and Geological digital Map Compilations of the South-Central Chile (36°-42°S), In: *The Andes active subduction orogeny*, Onken et al. editors, *Frontiers in Earth Sciences*, 565-568, Elsevier, 845 569p, [2006](#).
- Melnick, D., ~~& B. Bookhagen, B., M. Strecker, M., H. Echter, H., (2009).~~ Segmentation of megathrust rupture zones from fore-arc deformation patterns over hundreds to millions of years, Arauco Peninsula, Chile. *Journal of Geophysical Research*. 114. [10.1029/2008JB005788](https://doi.org/10.1029/2008JB005788), [2009](#).
- Menant, A., ~~S. Angiboust, S. T. Gerya, T. et al., (2020).~~ Transient stripping of subducting slabs controls periodic forearc uplift. *Nat Commun* 11, 1823. <https://doi.org/10.1038/s41467-020-15580-7>, [2020](#).
- 850 ~~Mendoza, C., S. Hartzel, S., and T. Monfret, T., (1994).~~ Wide-band analysis of the 3 March 1985 central Chile earthquake: Overall source process and rupture history, *Bull. Seismol. Soc. Am.*, 84, 269–283, [1994](#).
- Métois, M., ~~A. Socquet, A., C. Vigny, C., (2012).~~ Interseismic coupling, segmentation and mechanical behavior of the Central Chile subduction zone. *Journal of Geophysical Research*. 117. [10.1029/2011JB008736](https://doi.org/10.1029/2011JB008736), [2012](#).
- 855 Métois, M., Vigny, C., & Socquet, A. ~~(2016).~~ Interseismic Coupling, megathrust earthquakes and seismic swarms along the Chilean Subduction Zone (38°–18°S). *Pure and Applied Geophysics*, **173**, 1431–1449. <https://doi.org/10.1007/s00024-016-1280-5>, [2016](#).

Con formato: Español (Chile)

- Miller, N. C., ~~D.~~ Lizarralde, ~~D., J.A.~~ Collins, ~~J.A., W.S.~~ Holbrook, ~~W.S., H.J.~~ Van Avendonk, ~~H.J.~~, (2021). Limited mantle hydration by bending faults at the Middle America Trench. *Journal of Geophysical Research: Solid Earth*, 126, e2020JB020982. <https://doi.org/10.1029/2020JB020982>, 2021.
- 865 Moggi, K. (1977). Seismic activity and earthquake prediction, *Proc. Earthquake Pred. Res. Syrup.*, 1976, 203-214, Tokyo, 1977.
- Moggi, K., (1985). *Earthquake Prediction* (Academic Press, Tokyo-), 1985.
- Moreno, M., Rosenau, M., & Oncken, O. (2010). 2010 Maule earthquake slip correlates with pre-seismic locking of Andean subduction zone. *Nature*, 467, 198–202. <https://doi.org/10.1038/nature09349>, 2010.
- 865 Moreno, M., ~~D.~~ Melnick, ~~D., M.~~ Rosenau, ~~M., J.~~ Baez, ~~J., J.~~ Klotz ~~J., O.~~ Oncken, ~~O.,~~ et al., (2012). Toward understanding tectonic control on the Mw 8.8 2010 Maule Chile earthquake. *Earth and Planetary Science Letters*, 321, 152-165, 2012.
- Moreno, M., Haberland, C., Oncken, O. et al. Locking of the Chile subduction zone controlled by fluid pressure before the 2010 earthquake. *Nature Geosci* 7, 292–296 (2014).
- 870 Molina, D., ~~A.~~ Tassara, ~~A., R.~~ Abarca, ~~R., R.~~ D. Melnick, ~~R.D., A.~~ Madella, ~~A.,~~ (2021). Frictional segmentation of the Chilean megathrust from a multivariate analysis of geophysical, geological, and geodetic data. *Journal of Geophysical Research: Solid Earth*, 126, e2020JB020647, <https://doi.org/10.1029/2020JB020647>, 2021.
- Moscoco, E., ~~I.~~ Grevemeyer, ~~I.,~~ (2015). Bending-related faulting of the incoming oceanic plate and its effect on lithospheric hydration and seismicity: A passive and active seismological study offshore Maule, Chile. *Journal of Geodynamics*. 90. 58-70. 10.1016/j.jog.2015.06.007, 2015.
- 875 Mpodozis, C., ~~V.~~ Ramos, ~~V.,~~ (1990). The andes of Chile and Argentina. *Circum Pacific Council Publications*, 1990.
- Müller, R. D., ~~S.~~ Zahirovic, ~~S., S.E.~~ Williams, ~~S.E., J.~~ Cannon, ~~J., M.~~ Seton, ~~M., D.J.~~ Bower, ~~D.J., M.G.~~ Tetley, ~~M.G., C.~~ Heine, ~~C., E.~~ Le Breton, ~~E., S.~~ Liu, ~~S., S., S.H.J.~~ Russell, ~~S.H.J., T.~~ Yang, ~~T., J.~~ Leonard, ~~J., J., and M.~~ Gurnis ~~M.,~~ (2019). A global plate model including lithospheric deformation along major rifts and orogens since the Triassic. *Tectonics*, vol. 38,
- 880 2019.
- Nealy, J. L., ~~M.W.~~ Herman, ~~M.W., G.L.~~ Moore, ~~G.L., G.P.~~ Hayes, ~~G.P., H.M.~~ Benz, ~~H.M., E.A.~~ Bergman, ~~E.A., and S.E.~~ Barrientos, ~~S.E.,~~ (2017). 2017 Valparaíso earthquake sequence and the megathrust patchwork of central Chile, *Geophysical Research Letters* 44, doi: 10.1002/2017GL074767, 2017.
- Niemeyer, H., ~~H.~~ Berrios, ~~H., R.~~ de la Cruz, ~~R.,~~ (2004). Temperatures of formation in Triassic cataclasites of Cordillera Domeyko, Antofagasta, Chile. *Rev. Geol. Chile* 31, 3-18, 2004.
- 885 NOAA National Centers for Environmental Information (2022). ETOPO 2022 15 Arc-Second Global Relief Model. NOAA National Centers for Environmental Information. [Dataset]. DOI: 10.25921/fd45-gt74, 2022.
- Okada, Y. (1985). Surface Deformation due to Shear and Tensile Faults in a Half-Space. *Bulletin of the Seismological Society of America*, 75, 1135-1154, 1985.
- 890 Palacios, C., Ramírez, L.A., Townley, B., Solari, M., Guerra, N., (2007). The role of the Antofagasta–Calama Lineament in ore deposit deformation in the Andes of northern Chile. *Mineralium Deposita* 42, 301-308, 2007.

~~Pasten-Araya, F., P.-Salazar, P., S.-Ruiz, S., E.-Rivera, E., B.-Potin, B., A.-Maksymowicz, A., et al., (2018). Fluids along the plate interface influencing the frictional regime of the Chilean subduction zone, northern Chile. Geophysical Research Letters, 45. <https://doi.org/10.1029/2018GL079283>, 2018.~~

895 Peacock S.M., (1993). Large-scale hydration of the lithosphere above subducting slabs, Chemical Geology, Volume 108, Issues 1–4, Pages 49-59, ISSN 0009-2541, [https://doi.org/10.1016/0009-2541\(93\)90317-C](https://doi.org/10.1016/0009-2541(93)90317-C), 1993.

Pearce, R.K., A.-Sánchez de la Muela, A., M.-Moorkamp, M., J.O.S. Hammond, J.O.S., F.M.-Mitchell T.M., J.-Cembrano, J. Araya-Vargas, J., P.G.-Meredith, P.G., P.-Iturrieta, P., N.-Pérez-Estay, N., N.R.-Marshall, N.R., J.-Smith, J., G.-Yáñez, A.G., Griffith, A., W.-C.-Marquardt, C., A.-Stanton-Yonge, A., R.-Núñez, R., (2020). Reactivation of fault systems by compartmentalized hydrothermal fluids in the Southern Andes revealed by magnetotelluric and seismic data. Tectonics 39, e2019TC005997, 2020.

900

Peña, M., 2022. Origen de las Rotaciones Tectónicas en el Márgen Occidental de América del Sur: Influencia de Heterogeneidades en las Placas de Nazca y Sudamericana. Tesis para Optar al Grado de Doctor en Ciencias, Mención Geología. Inédito, 214 p. Universidad de Chile, Facultad de Ciencias Físicas Y Matemáticas, Departamento de Geología. Chile, 2022.

905 Perrin, C., Waldhauser, F., & Scholz, C. H. (2021). The shear deformation zone and the smoothing of faults with displacement. Journal of Geophysical Research: Solid Earth, 126, e2020JB020447. <https://doi.org/10.1029/2020JB020447>, 2021.

Philibosian, B., A.J.-Meltzer, A.J., (2020). Segmentation and supercycles: A catalog of earthquake rupture patterns from the Sumatran Sunda Megathrust and other well-studied faults worldwide. Quaternary Science Reviews 241, <https://doi.org/10.1016/j.quascirev.2020.106390>, 2020.

910 Poli P., A.-Maksymowicz, A., S.-Ruiz, S., The Mw 8.3 Illapel earthquake (Chile): Preseismic and postseismic activity associated with hydrated slab structures. Geology, 2017, 45 (3): 247–250. doi: <https://doi.org/10.1130/G38522.1>, 2017.

Piquer, J., Skármeta, J., Cooke, D.R., (2015). Structural evolution of the Río Blanco-Los Bronces district, Andes of central Chile: controls on stratigraphy, magmatism and mineralization. Economic Geology 110, 1995-2023, 2015.

915 Piquer, J., R.F. Berry, R.J. Scott, D.R. Cooke, (2016). Arc-oblique fault systems: their role in the Cenozoic structural evolution and metallogenesis of the Andes of central Chile. Journal of Structural Geology 89, 101–117, <https://doi.org/10.1016/j.jsg.2016.05.008>, 2016.

Piquer, J.; G.-Yáñez G., O.-Rivera O., D.-Cooke D., (2019). Long-lived damage zones associated with fault intersections in the Andes of Central Chile. Andean Geology 46 (2): [doi:<http://dx.doi.org/10.5027/andgeoV46n2-3106>], 2019.

920 Piquer J., O.-Rivera, O., G.-Yáñez, G., N.-Oyarzun, N., (2021a). The Piuquencillo Fault System: a long-lived, Andean-transverse fault system and its relationship with magmatic and hydrothermal activity, Solid Earth, (<https://doi.org/10.5194/se-2020-142>), 2021a.

Piquer, J., P.-Sanchez-Alfaro, P., P.-Pérez-Flores, P., (2021b). A new model for the optimal structural context for giant porphyry copper deposit formation. Geology 49, 597-601, <https://doi.org/10.1130/G48287.1>, 2021b.

925 Poli P., A.-Maksymowicz, A., S.-Ruiz, S., (2017). The Mw 8.3 Illapel earthquake (Chile): Preseismic and postseismic activity associated with hydrated slab structures. Geology, 45. 10.1130/G38522.1, 2017.

Con formato: Inglés (India)

Con formato: Inglés (India)



- Pritchard, M.E., ~~M. Simons, M., P.A. Rosen, P.A., S. Hensley, S., F.H. Webb, F.H., (2002)~~, Co-seismic slip from the 1995 July 30 Mw= 8.1 Antofagasta, Chile, earthquake as constrained by InSAR and GPS observations. *Geophysical Journal International*, 150: 362-376. <https://doi.org/10.1046/j.1365-246X.2002.01661.x>, 2002.
- Radic, J.P., ~~(2010)~~, Las cuencas cenozoicas y su control en el volcanismo de los Complejos Nevados de Chillán y Copahue-  
930 Callaqui (Andes del Sur, 36-39° S). *Andean Geology* 37 (1): 220-246. Doi: 10.5027/andgeoV37n1-a09, 2010.
- Ramos, V., ~~(2008)~~, The Basement of Central Andes: The Arequipa and Related Terranes. *Annu. Rev. Earth Planet. Sci.*, 36, pp. 289-324, 2008.
- Ramos, V., ~~S. Kay, S., (2006)~~, Overview of the tectonic evolution of southern central Andes of Mendoza and Neuquén (35°-39° S latitude). *Geological Society of America, Special Paper* 407, 2006.
- 935 Ranero, C., ~~& V., Sallares V., (2004)~~, Geophysical evidence for hydration of the crust and mantle of the Nazca plate during bending at the north Chile Trench. *Geology*. 32. 10.1130/G20379.1, 2004.
- Ranero, C. R., ~~A. Villaseñor, A., J. Phipps Morgan, J., and W. Weinrebe, W., (2005)~~, Relationship between bend-faulting at trenches and intermediate-depth seismicity, *Geochem. Geophys. Geosyst.*, 6, Q12002, doi:10.1029/2005GC000997, 2005.
- Ranero, C. R., Grevenmeyer, I., Sahling, H., Barckhausen, U., Hensen, C., Wallmann, K., Weinrebe, W., Vannucchi, P., von  
940 Huene, R., ~~& McIntosh, K., (2008)~~, Hydrogeological system of erosional convergent margins and its influence on tectonics and interplate seismogenesis. *Geochemistry, Geophysics, Geosystems*, 9, Q03S04. <https://doi.org/10.1029/2007GC001679>, 2008.
- Richards, J.P., Jourdan, F., Creaser, R.A., Maldonado, G., DuFrane, S.A., ~~(2013)~~, Geology, geochemistry, geochronology, and economic potential of Neogene volcanic rocks in the Laguna Pederal and Salar de Aguas Calientes segments of the Archibarca  
945 lineament, northwest Argentina. *Journal of Volcanology and Geothermal Research* 258, 47–73, 2013.
- Rivera, O., ~~2017~~, Geodynamic Setting for Porphyry Copper Deposits in Central Chile: Role of Translithospheric Structures and Gravimetric Anomalies in Andean Metallogeny. Master Thesis, Department of Geological Sciences, Faculty of Engineering and Geological Sciences. Catholic University of the North, Chile 215 pp, 2017.
- Rivera, O., ~~J. Cembrano, J., (2000)~~, Modelo de Formación de Cuencas Volcano-Tectónicas en Zonas de Transferencia  
950 Oblicuas a la Cadena Andina: El Caso de las Cuencas Oligo-Miocenas de Chile Central y su Relación con Estructuras WNW-NW (33°00' – 34°30' LS). In: 9º Congreso Geológico Chileno, Actas, vol. N°2, p. 631-636, Puerto Varas, 2000.
- Roquer, T., ~~G. Arancibia, G., J. Rowland, J., P. Iturrieta, P., D. Morata, D., J. Cembrano, J., (2017)~~, Fault-controlled development of shallow hydrothermal systems: structural and mineralogical insights from the Southern Andes. *Geothermics* 66, 156-173, <http://dx.doi.org/10.1016/j.geothermics.2016.12.003>, 2017.
- 955 Roland, E., ~~and J.J., McGuire, J.J., (2009)~~, Earthquake swarms on transform faults. *Geophysical Journal International*, 178: 1677-1690. <https://doi.org/10.1111/j.1365-246X.2009.04214.x>, 2009.
- ~~Ruegg, J.C., J. Campos, J., R. Armijo, R., S. Barrientos, S., P. Briole, P., R. Thiele, R., et al., (1996)~~, The Mw = 8.1 Antofagasta earthquake of July 30 1995: first results from teleseismic and geodetic data. *Geophys. Res. Lett.* 23 (9), 917–920, 1996.

Con formato: Italiano (Suiza)

Con formato: Inglés (India)

Con formato: Español (Chile)

Con formato: Español (Chile)

Con formato: Inglés (India)

Con formato: Inglés (India)

- 960 Ruiz, S., ~~R.~~Madariaga, ~~(2018)~~R.. Historical and recent large megathrust earthquakes in Chile. *Tectonophysics*.  
<http://dx.doi.org/10.1016/j.tecto.2018.01.015>, 2018.
- ~~Ruiz, S., R.~~Madariaga, ~~R.~~M. Astroza, ~~M.~~G.R. Saragoni, ~~G.R.~~M. Lancieri, ~~M.~~C. Vigny, ~~C.~~J. Campos, ~~J.~~(2012) Short  
 Period Rupture Process of the 2010 Mw 8.8 Maule Earthquake in Chile. *Earthquake Spectra*, Vol 28, N.S1, S1-S18, 2012.
- ~~Ruiz, S., M.~~Metois, ~~M.~~A. Fuenzalida, ~~A.~~J. Ruiz, ~~J.~~F. Leyton, ~~F.~~R. Grandin, ~~R.~~C. Vigny, ~~C.~~R. Madariaga ~~R.~~J.
- 965 Campos, ~~J.~~(2014). Intense foreshocks and a slow slip event preceded the 2014 Iquique Mw 8.1 earthquake. *Science*, 345,  
 1165-1169, DOI: 10.1126/science.1256074, 2014.
- Ruepke, L., ~~J.~~Morgan, ~~J.~~M. Hort, ~~M.~~J. Connolly, ~~J.~~(2004). Serpentine and the subduction water cycle. *Earth and Planetary  
 Science Letters*. 223. 17-34. 10.1016/j.epsl.2004.04.018, 2004.
- Salfity, J. A. ~~(1985)~~. Lineamentos transversales al rumbo andino en el Noroeste Argentino. In: IV Congreso Geológico  
 Chileno, Antofagasta, Chile, Vol. 2, pp. 119-137, 1985.
- 970 Saffer, D.M., & H. Tobin, ~~H.~~(2011). Hydrogeology and Mechanics of Subduction Zone Forearcs: Fluid Flow and Pore  
 Pressure. *Annu. Rev. Earth Planet. Sci.*. 39. 157-186. 10.1146/annurev-earth-040610-133408, 2011.
- Safer, D. M., ~~(2017)~~. Mapping fluids to subduction megathrust locking and slip behavior: Fluids and Subduction Megathrust  
 Locking, *Geophys Res Lett* 44, 9337-9340, 2017.
- 975 Sagripanti, L., Folguera, A., Gimenez, M., Rojas Vera, E.A., Fabiano, J.J., Molnar, N., Fennell, L., Ramos, V.A., ~~(2014)~~  
 Geometry of Middle to Late Triassic extensional deformation pattern in the Cordillera del Viento (Southern Central Andes): a  
 combined field and geophysical study. *J. Iber. Geol.* 40, 349-366, 2014.
- Saillard, M., ~~L.~~Audin, ~~L.~~B. Rousset, ~~B.~~J.P. Avouac, ~~J.P.~~M. Chlieh, ~~M.~~S. R. Hall, ~~S.R.~~J. Husson, ~~L.~~and D. L.  
 Farber, ~~D.L.~~(2017). From the seismic cycle to long-term deformation: linking seismic coupling and Quaternary coastal  
 geomorphology along the Andean megathrust, *Tectonics*, 36, doi:10.1002/2016TC004156, 2017.
- 980 Sandwell, D. T., Müller, R. D., Smith, W. H., Garcia, E., & Francis, R. ~~(2014)~~. New global marine gravity model from  
 CryoSat-2 and Jason-1 reveals buried tectonic structure. *Science*, 346(6205), 65-67, 2014.
- Santibáñez I., ~~J.~~Cembrano, ~~J.~~T. García-Pérez, ~~T.~~C. Costa, ~~C.~~G. Yáñez, ~~G.~~C. Marquardt, ~~C.~~G. Arancibia, ~~G.~~G.  
 González, ~~G.~~(2019). Crustal faults in the Chilean Andes: geological constraints and seismic potential, *Andean Geology*, 46  
 (1): 32-65. Doi: 10.5027/andgeoV46n1-3067, 2019.
- 985 Satake, K., ~~M.~~Heidarzadeh, ~~M.~~(2017). A Review of Source Models of the 2015 Illapel, Chile Earthquake and Insights from  
 Tsunami Data. In: Braitenberg, C., Rabinovich, A. (eds) *The Chile-2015 (Illapel) Earthquake and Tsunami*. Pageoph Topical  
 Volumes. Birkhäuser, Cham. [https://doi.org/10.1007/978-3-319-57822-4\\_1](https://doi.org/10.1007/978-3-319-57822-4_1), 2017.
- Scholz, C. H., ~~(1990)~~. *The Mechanics of Earthquakes and Faulting* (2<sup>nd</sup> Edition), Cambridge University Press, 504p, 1990.
- 990 Scholz, C. H., and J. Campos, ~~J.~~(2012). The seismic coupling of subduction zones revisited, *J. Geophys. Res.*, 117, B05310,  
 doi:10.1029/2011JB009003, 2012.

Con formato: Italiano (Suiza)

Con formato: Italiano (Suiza)

Con formato: Italiano (Suiza)

Con formato: Italiano (Suiza)

Con formato: Español (Chile)

Con formato: Español (Chile)

Con formato: Español (Chile)

Con formato: Español (Chile)

Con formato: Español (Chile)

Con formato: Inglés (India)

Schurr, B., G.-Asch, G., M.-Rosenau, M., R.-Wang R., O.-Oncken, O., S.-Barrientos, S., P.-Salazar, P., and J.-P., Vilotte, J.P., (2012). The 2007M7.7 Tocopilla northern Chile earthquake sequence: Implications for along-strike and downdip rupture segmentation and megathrust frictional behavior, *J. Geophys. Res.*, 117, B05305, doi:10.1029/2011JB009030, 2012.

995 Schurr, B., G.-Asch, G., S.-Hainzl, S., et al., (2014). Gradual unlocking of plate boundary controlled initiation of the 2014 Iquique earthquake. *Nature* 512, 299–302 <https://doi.org/10.1038/nature13681>, 2014

SERNAGEOMIN, (2003). Mapa Geológico de Chile 1:1.000.000: digital version. Servicio Nacional de Geología y Minería, Digital Geological Publication No. 4 (CD-ROM, version 1.0). Santiago, Chile, 2003.

1000 Shillington, D., A.-Bécel, A., M.-Nedimović, M., Et et al., (2015). Link between plate fabric, hydration and subduction zone seismicity in Alaska. *Nature Geosci* 8, 961–964. <https://doi.org/10.1038/ngeo2586>, 2015.

Sibson, R.H., (1990). Conditions for fault-valve behavior, in Knipe, R.J., and Rutter, E.H., eds., *Deformation Mechanisms, Rheology and Tectonics: Geological Society [London] Special Publication 54*, p. 15–28, <https://doi.org/10.1144/GSL.SP.1990.054.01.02>, 1990.

1005 Sibson, R.H., (2020). Preparation zones for large crustal earthquakes consequent on fault-valve action. *Earth, Planets and Space* 72:31, <https://doi.org/10.1186/s40623-020-01153-x>, 2020.

Sielfeld, G., D.-Lange D., J.-Cembrano, J., (2019). Intra-Arc Crustal Seismicity: Seismotectonic Implications for the Southern Andes Volcanic Zone, Chile. *Tectonics* 38, 552–578, <https://doi.org/10.1029/2018TC004985>, 2019.

1010 Stanton-Yonge, A., W.A.-Griffith, W.A., J.-Cembrano, J., R.-St. Julien, R., P.-Iturrieta, P., (2016). Tectonic role of margin-parallel and margin-transverse faults during oblique subduction in the Southern Volcanic Zone of the Andes: Insights from boundary element 43 modeling. *Tectonics* 35, 1990–2013, <https://doi.org/10.1002/2016TC004226>, 2016.

Talwani P., (2014). *Intraplate Earthquakes*, Cambridge University press, 360p, 2014.

Thingbaijam K. K. S., P.-M.-Mai, P.M., K.-Goda, K., (2017). New Empirical Earthquake Source-Scaling Laws. *Bulletin of the Seismological Society of America*; 107 (5): 2225–2246. Doi: <https://doi.org/10.1785/0120170017>, 2017.

1015 Torres, J., (2021). Caracterización del lineamiento Laguna fea-volcán san Pedro, región del Maule: Relación con actividad magmática e hidrotermal. Undergraduate thesis. Valdivia: Universidad Austral de Chile, 174, 2021.

Tsuji, T., J.-Ashi, J., Y.-Ikeda, Y., (2014). Strike-slip motion of a mega-splay fault system in the Nankai oblique subduction zone. *Earth Planet Sp* 66, 120. <https://doi.org/10.1186/1880-5981-66-120>, 2014.

1020 Vigny, C., A.-Socquet, A., S.-Peyrat, S., J.-C.-Ruegg, J.C., M.-Métois, M., R.-Madariaga, R., et al., (2011). The 2010 Mw 8.8 Maule Megathrust Earthquake of Central Chile, Monitored by GPS, *Science*, 1417-1421, 332, 6036, American Association for the Advancement of Science, doi: 10.1126/science.1204132, 2011.

Wall, R., P.-Gana, P., A.-Gutiérrez, A., (1996). Mapa Geológico del Área de San Antonio- Melipilla. Regiones de Valparaíso, Metropolitana y del Libertador Bernardo O'Higgins. Mapas Geológicos N°2, Escala 1:100.000. Sernageomin, Chile, 1996.

Wall, R., D.-Sellés, D., P.-Gana, P., (1999). Geología del Área Títil-Santiago, Región Metropolitana de Santiago. Serie Mapas Geológicos N°11, Escala 1:100.000. Sernageomin, Chile, 1999.

Código de campo cambiado

Con formato: Español (Chile)

Con formato: Inglés (India)

Con formato: Inglés (India)

Con formato: Inglés (India)

Con formato: Inglés (India)

- 025 Wallace, L. M., Beavan, J., McCaffrey, R., & Darby, D., ~~(2004)~~. Subduction zone coupling and tectonic block rotations in the North Island, New Zealand. *Journal of Geophysical Research*, **109**, B12406. <https://doi.org/10.1029/2004JB003241>, 2004.
- Wang, K., & ~~S.L.~~ Bilek, ~~S.L.~~, ~~(2011)~~. Do subducting seamounts generate or stop large earthquakes? *Geology* 39, 819–822.
- Wdowinski, S., (1992). Dynamically supported trench topography. *J. Geophys. Res.*, 97( B12), 17651– 17656, doi:10.1029/92JB01337, 2011.
- 030 Wiemer, D., Hagemann, S.G., Hayward, N., Begg, G.C., Hronsky, J., Thébaud, N., Kemp, A.I.S., Villanes, C., ~~(2023)~~. Cryptic trans-lithospheric fault systems at the western margin of South America: implications for the formation and localization of gold-rich deposit superclusters. *Frontiers in Earth Science* 11, 1159430, doi: 10.3389/feart.2023.1159430, 2023.
- Xia, S., ~~J.~~ Sun ~~J.~~, ~~H.~~ Huang, ~~H.~~, ~~(2015)~~. Degree of serpentinization in the forearc mantle wedge of Kyushu subduction zone: quantitative evaluations from seismic velocity. *Marine Geophysical Research*, 36, 101-112, 2015.
- 035 Yáñez-Cuadra, V., Ortega-Culaciati, F., Moreno, M., Tassara, A., KrummNualart, N., Ruiz, J., et al. ~~(2022)~~. Interplate coupling and seismic potential in the Atacama Seismic Gap (Chile): Dismissing a rigid Andean sliver. *Geophysical Research Letters*, 49, e2022GL098257. <https://doi.org/10.1029/2022GL098257>, 2022.
- Yáñez, G., ~~P.~~ Gana, ~~P.~~, ~~R.~~ Fernández, ~~R.~~, ~~(1998)~~. Sobre el origen y significado geológico de la anomalía Melipilla, zona central de Chile. *Revista Geológica de Chile*, 25, No. 2, 175-198, 1998.
- 040 Yáñez, G., ~~C.R.~~ Ranero, ~~C.R.~~, ~~R.~~ Von Huene, ~~R.~~, ~~J.~~ Díaz, ~~J.~~, ~~(2001)~~. Magnetic anomaly interpretation across the southern central Andes (32°-34°S): The role of the Juan Fernandez Ridge in the late Tertiary evolution of the margin. *Journal of Geophysical Research*. 106, 6325-6345, 2001.
- Yáñez, G., ~~J.~~ Cembrano, ~~J.~~, ~~(2004)~~. The role of the viscous plate coupling in the late tertiary Andean deformation. *Journal of Geophysical Research*, vol 106, 6325-6345, 2004.
- 045 Yáñez, G., ~~O.~~ Rivera, ~~O.~~, ~~(2019)~~. Crustal dense blocks in the fore-arc and arc region of Chilean ranges and their role in the magma ascent and composition. *Breaking paradigms in the Andean metallogeny*, *Journal of South American Earth Sciences*, 93, pp. 51-66. DOI: 10.1016/j.jsames.2019.04.006, 2019.
- Yue, L.T., ~~E.~~ Brodsky, ~~E.~~, ~~C.~~ An, ~~C.~~, ~~(2014)~~. The 1 April 2014 Iquique, Chile, Mw 8.1 earthquake rupture sequence, *Geophys. Res. Lett.*, 41, 3818– 3825, doi:10.1002/2014GL060238, 2014.
- 050 Zienkiewicz, O. C., and ~~R.L.~~ Taylor, ~~R.L.~~, ~~(1991)~~. *The Finite Element Method*, vol. 2, *Solid and Fluid Mechanics Dynamics and Non-linearity*, 4th ed., McGraw-Hill, New York, 1991.

Con formato: Español (Chile)

Con formato: Español (Chile)

Con formato: Español (Chile)

Con formato: Español (Chile)

Con formato: Inglés (India)